Supplementary Information

Microbial dormancy under freeze–thaw cycling regulates alpine soil responses to warming

Shanshan Qi[1], Gangsheng Wang[1,*], Shuhao Zhou[1], Daifeng Xiang[1], Zirui Mu[1], Wanyu Li[1], Zehao Lv[1], Biao Zhu[2,3], Jin-Sheng He[2,4]

[1]State Key Laboratory of Water Resources Engineering and Management, and Institute for Water-Carbon Cycles and Carbon Neutrality, Wuhan University, Wuhan, 430072, China

[2]State Key Laboratory for Vegetation Structure, Function and Construction (VegLab), Ministry of Education Key Laboratory for Earth Surface Processes, and College of Urban and Environmental Sciences, Peking University, Beijing, China

[3]Ministry of Education Key Laboratory for Ecology and Resource Use of the Mongolian Plateau, Inner Mongolia Key Laboratory for Grassland Ecology, and School of Ecology and Environment, Inner Mongolia University, Huhhot, China

[4]State Key Laboratory of Herbage Improvement and Grassland Agro-ecosystems, and College of Pastoral Agriculture Science and Technology, Lanzhou University, Lanzhou, China

[*]Corresponding author:

Gangsheng Wang, wanggs@whu.edu.cn, ORCID: 0000-0002-8117-5034

Supplementary Text

1. Microbial-ENzyme Decomposition (MEND) model with freeze-thaw processes

1.1 Model description

The MEND model (see Fig. 1a in main text) [1, 2, 3] allows for mechanistic representation of (i) density-based partitioning and physicochemical protection of soil organic matter (SOM); (ii) distinct microbial and enzyme groups regulating SOM decomposition and inorganic nitrogen (N) transformations including N mineralization & immobilization, biological N fixation, nitrification, and sequential denitrification; (iii) microbial physiology such as growth & maintenance, dormancy & resuscitation, and mortality in response to changes in soil pH, temperature, and moisture; (iv) plant-microbial competition for inorganic N (NH_4^+ and NO_3^-); (v) ammonium (NH_4^+) sorption and nitrate (NO_3^-) & nitrite (NO_2^-) leaching; and (vi) N gases (NO, N_2O, and N_2) exchange between soil and the atmosphere.

The MEND model with freeze-thaw processes (MEND-FT) explicitly incorporates freeze-thaw processes in permafrost and seasonally frozen soils, along with corresponding responses of soil biogeochemical and microbial-enzymatic functions. Model state variables, governing equations, component fluxes and parameters are described in Supplementary Table S1–S5.

1.1.1. Soil carbon (C) and nitrogen (N) pools

The MEND model includes the following soil C-N pools (Table S1):

Five SOM (with both C & N) pools: particulate organic matter (POM) decomposed by oxidative enzymes (POM_O), POM decomposed by hydrolytic enzymes (POM_H), mineral-associated organic matter (MOM), dissolved organic matter (DOM), and active MOM (QOM) interacting with DOM via sorption and desorption.

Seven inorganic N pools: adsorbed ammonium (NH_4^+ Adsorb), non-adsorbed ammonium (NH_4^+), nitrate (NO_3^-), nitrite (NO_2^-), nitric oxide (NO), nitrous oxide (N_2O), and dinitrogen (N_2).

Two microbial (with both C & N) functional groups: active and dormant microbes (MB_A and MB_D).

Three enzyme functional groups for SOM decomposition: POM_O-degrading enzymes (EP_O), POM_H-degrading enzymes (EP_H), and MOM-degrading enzymes (EM).

Six enzymes as bioindicators controlling inorganic N transformations: nitrogenases (corresponding to functional genes of *nifH*), ammonia oxidases (*amoA* & *nxrA/B*), nitrate reductases (*narG/napA*), nitrite reductases (*nirS/nirK*), nitric oxide reductases (*norB*), and nitrous oxide reductases (*nosZ*) [4, 5].

The governing (C or N mass balance) equations for these C-N pools are summarized in Table S2, where Eq. S11 shows the overall soil C mass balance and Eqs. S21a–c indicates the mass balance of soil organic N, inorganic N, and total N, respectively.

1.1.2. Flexible stoichiometry

In contrast to traditional models that use fixed SOM C:N ratios [6, 7], we use flexible stoichiometry (i.e., time-variant C:N ratio) for SOM and microbial biomass pools to represent the adaption of microbes in response to the stoichiometric imbalance of available resources [8, 9, 10, 11, 12]. One exception is for the enzyme pools, where a fixed C:N ratio (=3) is used according to Schimel and Weinstraub [13]. Generally, the organic N flux will follow the organic C flux according to the C:N ratio in the upstream (source) pool (see Eq. S14 in Table S2). The C:N ratios in the SOM pools (including POM_O, POM_H, MOM, QOM, DOM) will be regulated by the litter input, C-N flux from upstream pool, and/or microbial turnover. The C:N ratio in the microbial biomass pool is self-regulated by the DOM uptake, heterotrophic respiration (R_h), N mineralization and immobilization. R_h is mainly controlled by the intrinsic C use efficiency (Y_g or intrinsic CUE) (see Eqs. S33–S37 in Table S3). In addition to the availability of DON and inorganic N (NH_4^+ and NO_3^-), we define an intrinsic N use efficiency (YN_g or intrinsic NUE, see Eq. S47 in Table S4) to modify N mineralization rate (Eq. S46 in Table S4) and

immobilization rates (Eqs. S48–S49). In Eq. S47, we first assume a conservative C:N range (i.e., between $CN_{BA,min}$ and $CN_{BA,max}$) to represent the stoichiometric plasticity of microbial communities [8, 12, 14]. Intrinsic NUE (YN_g in Eq. S47) will increase with increasing microbial C:N ratio (CN_{BA}), with YN_g being 0 when $CN_{BA} \leq CN_{BA,min}$ (C-limited) and YN_g approaching 1 when $CN_{BA} \geq CN_{BA,max}$ (N-limited). This means that N mineralization rate will decrease, and N immobilization rate will increase when microorganisms become more N limited, resulting in higher YN_g [11].

1.1.3. SOM decomposition

The decomposition of POM_O, POM_H, and MOM pools is modeled by the Michaelis-Menten kinetics [15, 16]. The decomposition flux is determined by the concentration of a SOM pool and its corresponding enzymes (e.g., POM_O and EPo), as well as two kinetic parameters, i.e., the specific enzyme activity and the half-saturation constant (Vd and K) (see Eqs. S24–S26 in Table S3).

1.1.4. DOM sorption and desorption

The sorption and desorption between DOM and QOM are simultaneously considered as dynamic processes [3]. DOM adsorption is controlled by DOM concentration and mineral surface coverage, and desorption is presumed to only depend on surface coverage (Eqs. S27–S28 in Table S3). Relative saturation of the QOM pool (i.e., Q/Q_{max}, ratio of actual adsorbed C content to the sorption capacity) is defined to represent the fraction of the mineral surface area occupied [3].

1.1.5. Microbial growth, maintenance, and mortality

Microbial growth and maintenance are described by the Compromise model that combines the features of the Pirt model and the Herbert model [17]. The Compromise model explicitly

expresses the dependence of microbial maintenance on both microbial biomass and substrate (DOM) availability (Eqs. S29, S33–S34 in Table S3). We define a parameter ($\alpha = V_m /(V_g + V_m) \leq 0.5$) to constrain the relationship between the maximum specific growth and maintenance rate (V_g and V_m) (Eq. S29). The maintenance rate of dormant microbes is much lower than that of active microbes by a factor of β = 0.001–0.01 (Eq. S36) [1]. Microbial mortality rate ($\gamma \cdot V_m$ in Eq. S32) is associated with the maintenance rate by a scaling factor (γ).

1.1.6. Microbial dormancy and resuscitation

When environmental conditions are unfavorable for growth, microbes may enter a state of low metabolic activity (i.e., dormancy) until conditions improve to allow replication [18, 19]. We simulate microbial dormancy and resuscitation as reversible dynamic processes (Eqs. S30–S31 in Table S3), which are mainly determined by the availability of DOM and soil moisture.

1.1.7. Competitive dynamic enzyme allocation and turnover

We propose a COmpetitive Dynamic Enzyme Allocation (CODEAL) scheme to deal with the synthesis of multiple enzymes (e.g., eight groups in this study). The enzyme allocation approach developed here is based on the synthetic results that enzyme activities are dependent on microbial biomass [20] and substrate availability [21]. The synthesis of SOM-degrading enzymes (EP_O, EP_H and EM) depends upon the active microbial biomass and the relative abundance of the C substrate that needs to be decomposed (Eq. S38) [1]. Given that the synthesis of SOM-degrading enzymes has been calculated in advance, the total synthesis rate of all inorganic-N enzymes is assumed to be proportional to the total synthesis rate of all SOM-degrading enzymes by a scaling factor, which is defined as the ratio of total soil inorganic N to total soil organic N ($(NH4 + NO3 + NO2)/\sum_{i=1}^{4} SON_i$) (Eq. S40). A competitive allocation scheme is applied to the production of enzymes for each inorganic-N transformation process, where the competitive

allocation coefficient is the saturation level of an inorganic N substrate (i.e., N_j/KSN_j, the ratio of the substrate concentration to the half-saturation constant) compared to the overall saturation level of all inorganic N substrates ($\sum_{j=1}^{6}\left(N_j/KSN_j\right)$) (Eq. S40). Enzyme turnover is proportional to the enzyme concentration by the turnover rate (Eqs. S39 and S41). The turnover of extracellular enzymes (EP_O, EP_H and EM) enters the DOM pool, whereas the turnover of intracellular enzymes (nitrogenase, ammonia oxidases, and N-reductases) becomes microbial biomass, as these N-enzymes are located at cell membrane, cytoplasm, or periplasm [22, 23, 24].

1.1.8. Soil respiration

MEND simulates soil respiration (Rs) as the sum of autotrophic (root) respiration (R_a) and heterotrophic (microbial) respiration (R_h), where R_a is calculated as a fraction ($f_{Ra} \in (0.1,0.4)$) of gross primary production (GPP, g C m^{-2} d^{-1}); and R_h is the sum of microbial growth respiration ($R_{h,g}$), maintenance respiration ($R_{h,g}$), and overflow respiration ($R_{h,g}$) (see Eqs. S10–S12 in Table S2 and Eqs. S33–37 in Table S3. Microbes may release CO_2 via overflow respiration to make the microbes meet their stoichiometry constraint (i.e., maximum allowed microbial C:N ratio) [25, 26].

1.1.9. Microbial N mineralization and plant-microbial competition for inorganic N

Based on our definition of intrinsic NUE (YN_g in Eq. S47), a fraction (YN_g) of ingested DON is incorporated into microbial biomass and the rest is mineralized (Eq. S46). We adapted the Equilibrium Chemistry Approximation (ECA) kinetics [27] to model the plant-microbial competition for inorganic N (NH_4^+ and NO_3^-) (Eqs. S48–S52).

1.1.10. Biological N fixation, nitrification, and denitrification

The biological N fixation (BNF), nitrification, and denitrification processes are simulated via the Michaelis-Menten kinetics, with each reaction being mediated by the corresponding

enzyme groups. The BNF rate is also modified by the soil NH_4^+ availability (quantified by the saturation level of NH_4^+), i.e., higher soil NH_4^+ availability will inhibit N fixation (Eq. S45) [28]. The nitrification and denitrification chain reactions ($NO_3^- \rightarrow NO_2^- \rightarrow NO \rightarrow N_2O \rightarrow N_2$) are catalyzed by specific enzymes (Eqs. S42 and S44). In addition, nitrifier-denitrification flux is modeled as a fraction of the nitrification flux and contributes to N_2O production [29, 30], where the fraction is controlled by oxygen availability (Eq. S43).

1.1.11. Ammonium (NH_4^+) sorption and nitrate (NO_3^-) & nitrite (NO_2^-) leaching

We also consider the sorption of NH_4^+ using the Langmuir isotherm model (Eq. S53) [31]. Only the un-adsorbed NH_4^+ is available for microbial and plant uptake. The leaching of NO_3^- and NO_2^- is controlled by the concentration of NO_3^- and NO_2^- in soil solution as well as the amount of soil water percolation (Eq. S54) [32].

1.1.12. N gases (NO, N_2O, and N_2) exchange between soil and the atmosphere

N gases exchange between soil and the atmosphere is simulated by a diffusion process governed by the Fick's law (Eq. S55), i.e., the flux is mainly determined by the difference in gas concentrations between soil and the atmosphere as well as the gas diffusivity in soil. Gas diffusivity is dynamically calculated by internal and external air-filled porosities in bimodal (aggregated) soil porous media [33, 34, 35].

1.2. Soil freeze-thaw processes and environmental responses

1.2.1 Soil freeze-thaw processes in cold regions

We employed a daily time step to simulate the freeze-thaw processes. The specific computational procedure was as follows: (i) identified soil freeze and thaw phases based on

daily soil temperature data; (ii) calculated the frozen depth (*zFrozen*) and thawed depth (*zThaw*) using the Stefan equation (see Eq. 5 in main text) [36, 37]; and (iii) determined the distribution of the freeze-thaw process by accounting for site-specific freezing types (Fig. S1) [38]. The classification of freeze and thaw phases, as well as the calculation of frozen and thawed depth, are described in the section "Freezing and thawing fronts calculation" in main text. Site-specific freezing types include seasonally frozen soils and permafrost regions (Fig. S1). In seasonally frozen soils, the calculated maximum thawed depth was typically greater than the maximum frozen depth. As a result, the maximum frozen depth kept unchanged until the thawed depth reached or exceeded the frozen depth, after which the whole-soil thawed until the onset of the next freezing phase (Fig. S1). In permafrost regions, the opposite pattern was observed, where frozen depths generally dominate, and the computational logic was accordingly reversed (Fig. S1).

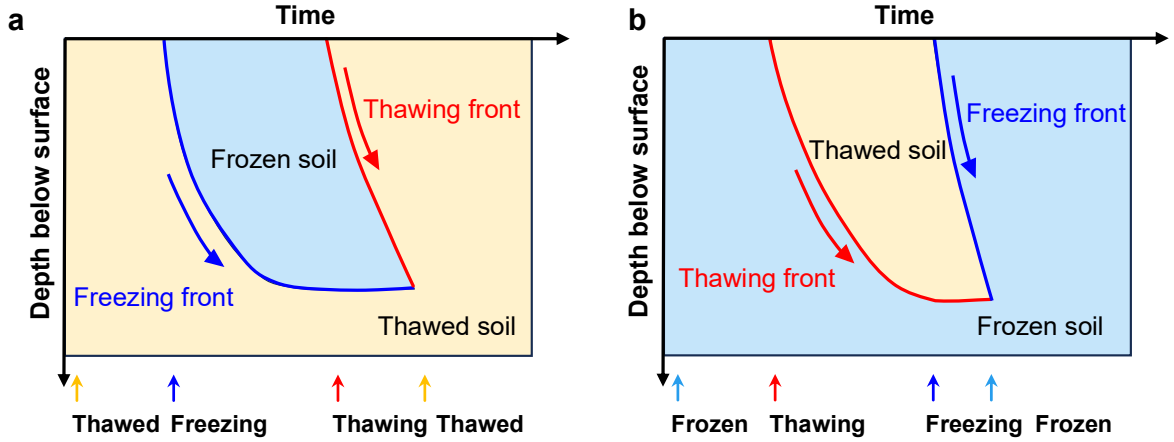

Fig. S1 | Conceptual progression of freezing and thawing fronts during a freeze-thaw cycle in (a) seasonally frozen soils and (b) permafrost regions.

1.2.2 Response functions for freeze-thaw dynamics

The freeze-thaw responses follow a hyperbolic function, incorporating the site-specific

distribution of substrate within the soil profile [39, 40]. This is because the relative thawed soil layer, or active layer thickness (ALT), determines how much substrate is released and thus available to microbes [41, 42]. We represent the relative thawed proportion using a dimensionless scaling factor, ALTscalar, defined as the ratio of the thawed soil depth to the total soil depth. This factor is calculated based on the positions of freezing and thawing fronts relative to soil depth (see Eq. S59 in Table S6). The soil freeze-thaw response functions are summarized in Table S6. In the MEND-FT model, the reaction rate may be modified by freeze-thaw processes and/or environmental conditions (i.e., soil pH, temperature and moisture, see the following section for details) (Eqs. S57–S58 in Table S6).

The response function for SOM decomposition and inorganic N transformations, f_{dec}(ALTscalar) (Eq. S60 in Table S6), is derived from empirical analyses [39, 40]. The parameter a (*ALTa* in Table S5) is a shape parameter that controls the distribution of available substrate. We adopted $a = 0.54$ from Liu, Zhuang [40], which was estimated using observation data in alpine meadow sites on the Qinghai-Tibetan Plateau. A minimum response function value, f_{dec}(ALTscalar)_min, accounts for site-specific SOC distribution to represent substrate availability in deep unfrozen soils [43]. In this study, we assigned f_{dec}(ALTscalar)_min = 0.15 [40].

The response functions for microbial dormancy (f_{A2D}(ALTscalar), Eq. S61 in Table S6) and resuscitation (f_{D2A}(ALTscalar), Eq. S62 in Table S6) follow a pattern similar to substrate accessibility (see relevant section in main text). The parameter b (*ALTb* in Table S5) shapes these response functions. We set $b = 1.11a$ to account for the slightly reduced response following thawing, due to physiological recovery and delays in substrate diffusion [44, 45]. In fully

frozen soils, a small proportion of microbes remains active, and resuscitation persists at a very low rate [46]. Similarly, some microbes may enter dormancy even when the soil is totally thawed [47]. Accordingly, we define minimum microbial dormancy response (f_{A2D}(ALTscalar)_min) or resuscitation response (f_{D2A}(ALTscalar)_min), which ranges from 0.01 to 0.2 (parameter *ALTc* in Table S5).

1.2.3 Soil pH, temperature and moisture response functions

The pH response function, $f(pH)$, follows an exponential-quadratic function (Eq. S63 in Table S6) [48]. The temperature sensitivity of true growth yield or intrinsic carbon use efficiency (Y_g) is modeled by a linear function (Eq. S64 in Table S6) [49, 50, 51, 52, 53, 54]. The Arrhenius equation (Eq. S65) or Q_{10} method (Eq. S66) is used to simulate the response of other parameters [3] to changes in temperature. The relationship between Q_{10} and Ea (Eq. S67) is derived from Eqs. S65 and S66. The activation energy (Ea) for selected parameters is described in Wang et al., [3]. We use different soil moisture response functions (SMRFs) [2] to describe the influences of soil moisture on the enzyme-mediated SOM decomposition processes, microbial mortality, microbial dormancy and resuscitation, nitrification and denitrification:

(1) The SMRF for SOM decomposition by oxidative enzymes (Eq. S68 in Table S6) is adapted from Hansen et al. [55].

(2) The SMRF for SOM decomposition by hydrolytic enzymes (Eq. S69 in Table S6) is based on Manzoni et al. [56]. The values of ψ_{min} and b in Eq. S69 for soil or litter in different biomes were adapted from Manzoni *et al*. [56].

(3) The SMRFs for microbial mortality, dormancy & resuscitation are also shown (Eqs. S70 and S71 in Table S6). Soil water potential greatly affects the microbial dormancy and reactivation processes and various sigmoidal-type switching functions have been proposed to quantify these effects [2, 57]. The response functions (Eqs. S70 and S71 in Table S6) are used to modify the dormancy ($f_{A2D}(\psi)$) and the reactivation ($f_{D2A}(\psi)$), where ψ is the SWP (MPa) and the exponent ω describes the steepness of the curve; ψ_{A2D} and ψ_{D2A} are critical SWPs depending on the osmolyte synthesis strategy; and τ is the ratio between ϕ_{D2A} and ϕ_{A2D} and is less than 1 to capture a lagged switch from dormant to active state upon rewetting [57]. We also use $f_{A2D}(\psi)$ to modify microbial mortality rate.

(4) The SMRFs for nitrification and denitrification (Eq. S72 in Table S6). The values for WFP_i, $(i = 1,2,3,4)$ and a_+, b_+, a_-, b_- are adapted from Muller [58] and Wang & Chen [35].

2. Model Initialization and Input Data

2.1. Model initialization

We initialized the C-N pool sizes using experimentally measured values [59]. When data were not available, initial soil and enzyme pool sizes were estimated based on literature sources. For example, MOC typically accounts for 40–50% of SOC, and the POC to MOC ratio is approximately 1.0–1.5 at the Haibei site [60]. Enzyme concentrations are around 0.1–1% of MBC [1, 48].

2.2. Model input data

Model input data are used to drive model simulations and generally include: (i) litter input or GPP; (ii) soil pH, temperature and moisture; (iii) inorganic N (NH_4^+ and NO_3^-) input (e.g.,

dry/wet deposition and fertilization). Depending on the data availability, these input data may be provided as constant values or time-variant values at hourly, daily, monthly scale. All input data will be automatically interpolated or converted to hourly data for MEND model simulations. Soil texture and/or soil water retention curve parameters for the van Genuchten model [61, 62] are also needed for modeling, where the soil water retention curve is used to convert volumetric water contents to soil water potentials [2, 63]. In this study, data input included daily soil temperature and moisture, as well as GPP under both control and warming treatments (see Section "Study site and data compilation" in main text). Soil pH was held constant at 8.4 for treatments [59].

2.3. Whole-soil warming experimental data

The experimental data for this study were obtained from published research [59, 64] conducted at a seasonally frozen alpine meadow site on the northeastern QTP. Briefly, the warming experiment consists of four blocks, each containing one control plot and one warming plot (+ 4℃ at 0–100 cm soil depth). The experiment began in June 2018 and data were recorded through September 2021. Soil CO_2 flux (soil respiration) was measured on seven dates in 2018, ten dates in 2019 and 2020, and five dates in 2021 during the growing seasons (May to September). Measurements of SOC, MBC, microbial C:N and inorganic N (NH_4^+ and NO_3^-) were taken at the end of August in 2019 and 2021 [59]. Microbial carbon use efficiency (CUE) and enzyme activities for oxidases and hydrolases were assessed in August 2021 [64].

3. Model Parameterization, Calibration and Validation

3.1. Model parameterization procedure

A rigorous model parameterization procedure is essential to avoid methodological

problems in the subsequent model calibration and validation. We adopt the following procedure for model parameterization [65, 66]: (i) The parameter classes are determined based on site properties such as soil texture or types, plant functional types, and climatic zones, so that the parameter values in different classes could be assessable from available field data. (ii) The number of practically calibrated parameters should be kept as low as possible. This means to calibrate the most important and sensitive parameters and the other parameters should be fixed based on previous studies. (iii) For the parameters subjected to calibration, physically, chemically, or biologically acceptable intervals for the parameter values are summarized in Table S5.

3.2. Multi-objective parameter sensitivity analysis

Sensitivity analysis is used to identify important model parameters for model-data integration. We developed a Multi-Objective Parameter Sensitivity Analysis (MOPSA) method based on the Wilcoxon Rank Sum Test [67]. The MOPSA can be used to identify the relative importance of each model parameter for each objective or response variable (e.g., a C or N pool or flux). The sensitivity is characterized by the difference in the probability distribution between two (i.e., acceptable and unacceptable) parameter samples that are separated by a threshold of the objective functional values in terms of a specific response variable. The difference is statistically quantified by the Wilcox estimator from the non-parametric Wilcoxon Rank Sum Test, which is more applicable to statistical analysis of difference in parameters that are often not normally distributed [67]. This Wilcox estimator is then used as the sensitivity index to quantify the magnitude of parameter sensitivity, i.e., higher sensitivity index means higher

sensitivity. The Wilcox-based Multi-Objective Parameter Sensitivity Analysis (MOPSA) approach consists of the following steps:

(i) Generating parameter samples. Select the parameters to be evaluated and generate parameter sets in terms of their ranges using the sample generator in the MOEA Framework [68].

(ii) Running MEND model to calculate objective function values. Run MEND with these parameter sets and compute the objective function values in terms of response variables (e.g., C or N pools or fluxes). The objective function is defined as the mean squared error (MSE) between simulated and reference time-series data. The simulated data are the simulated pool sizes or fluxes using a generated parameter set. the reference data refer to model-simulated pool sizes or fluxes using the medians of parameters.

(iii) Identifying acceptable and unacceptable parameter sets. For each response variable, identify whether a parameter set is acceptable or unacceptable by comparing the MSE to a given criterion, e.g., the 50% divisions of the sorted MSE. The MSE less than the criterion is classified as acceptable, otherwise it is classified as unacceptable.

(iv) Normalizing the parameter values by their value ranges. For the *i*th parameter, let $X_i = \{x_{i,j}, j = 1,2,\cdots,2n\}$ be the parameter values. Define $x_{i,\min} = \min\{X_i\}$ and $x_{i,\max} = \max\{X_i\}$, and the normalized X_i, denoted by $Z_i = \{z_{i,j}, j = 1,2,\cdots,2n\}$ is defined as $z_{i,j} = \frac{x_{i,j} - x_{i,\min}}{x_{i,\max} - x_{i,\min}} \in [0,1]$. Let $Z_i^A = \{z_{i,j}^A, j = 1,2,\cdots,n\}$ and $Z_i^U = \{z_{i,j}^U, j = 1,2,\cdots,n\}$ be the subsets of acceptable and unacceptable Z_i (i.e., normalized X_i), respectively. The normalization of parameter values makes the sensitivity index comparable between different parameters.

(v) Conducting the Wilcox test to determine parameter sensitivity. Implement the Wilcox test of the two parameter samples, i.e., Z_i^A and Z_i^U. The Wilcox estimator for the difference between acceptable and unacceptable parameters is used as the sensitivity index to quantify the magnitude of parameter sensitivity, i.e., higher sensitivity index means higher sensitivity. The *p-value* from the Wilcox test is used to evaluate if the parameter sensitivity is statistically significant ($p < 0.05$) or not ($p \geq 0.05$). Note that the Wilcox estimator refers to the median of the difference between acceptable and unacceptable parameter samples [67].

3.3. Multi-objective functions for model calibration and validation

We calibrate selected model parameters (Table S5) by achieving high goodness-of-fits of model simulations against experimental observations. We implement multi-objective calibration of the model [1, 2, 69]. Each objective evaluates the goodness-of-fit of a specific observed variable mentioned above. The parameter optimization is to minimize the overall objective function (J) that is computed as the weighted average of multiple single-objectives [66].

$$J = \sum_{i=1}^{m} w_i \cdot J_i \tag{S73a}$$

$$\sum_{i=1}^{m} w_i = 1 \text{ and } w_i \in [0,1] \tag{S73b}$$

where m denotes the number of objectives and w_i is the weighting factor for the i^{th} (i = 1,2,…, m) objective function (J_i).

The individual objective function J_i may be calculated as (1− R^2), |PBIAS|, MARE, MAREt, or (1−r):

$$R^2 = 1 - \frac{\sum_{i=1}^{n}[Y_{sim}(i) - Y_{obs}(i)]^2}{\sum_{i=1}^{n}[Y_{obs}(i) - \bar{Y}_{obs}]^2} \tag{S74}$$

$$|\text{PBIAS}| = \left|\frac{\bar{Y}_{sim} - \bar{Y}_{obs}}{\bar{Y}_{obs}}\right| \tag{S75}$$

$$\mathrm{MARE} = \frac{1}{n}\sum_{i=1}^{n}\left|\frac{Y_{sim}(i)-Y_{obs}(i)}{Y_{obs}(i)}\right| \quad \text{(S76)}$$

$$\mathrm{MAREt} = \begin{cases} 0, & \mathrm{MARE} \le tolerance \\ \mathrm{MARE}, & \mathrm{MARE} > tolerance \end{cases} \quad \text{(S77)}$$

$$r = \frac{\sum_{i=1}^{n}[Y_{obs}(i)-\bar{Y}_{obs}]\cdot[Y_{sim}(i)-\bar{Y}_{sim}]}{\sqrt{\sum_{i=1}^{n}[Y_{obs}(i)-\bar{Y}_{obs}]^2}\cdot\sqrt{\sum_{i=1}^{n}[Y_{sim}(i)-\bar{Y}_{sim}]^2}} \quad \text{(S78)}$$

where R^2 denotes the coefficient of determination; |PBIAS| is the percent bias between simulated and observed mean values; MARE is the Mean Absolute Relative Error (MARE) and represents the averaged deviations of simulations (Y_{sim}) from their observations (Y_{obs}); *MAREt* is a variant of MARE and MAREt achieves the best (= 0) when MARE is within a defined tolerance value; *r* is the Pearson correlation coefficient; *n* is the number of data; Y_{obs} and Y_{sim} are observed and simulated values, respectively; and $\bar{Y}_{obs}$ and $\bar{Y}_{sim}$ are the mean value for Y_{obs} and Y_{sim}, respectively.

Different objective functions are used to quantify the goodness-of-fit for different variables, depending on the measurement method and frequency of variables. R^2 quantifies the proportion of the variance in the response variables that is predictable from the independent variables [2]. A higher R^2 ($R^2 \le 1$) indicates better model performance. R^2 is used to evaluate the variables (e.g., total soil respiration or heterotrophic respiration) that are frequently measured, and the absolute values can be directly compared between observations and simulations. MARE or |PBIAS| is used to evaluate the variables (e.g., microbial biomass C and concentrations of inorganic N) with only a few measurements and the absolute values can be directly compared. Lower MARE or |PBIAS| values (≥ 0) are preferred [2, 70]. MAREt should be used when the simulated value may not be necessarily to strictly match the observed or measured value. For example, the measured nitrification rates are more like potential rates or rough estimates. It is more appropriate to use MAREt to evaluate the model simulated actual nitrification rates when compared with these measurements. Another example includes the comparison between simulated and observed N fixation or plant N uptake rates. The observations collected from

literature just represent empirical or reference N fixation [71] or plant N uptake rates [72, 73]. In this case, we also recommended to use MAREt as we expected the simulated N fixation or plant N uptake rates would fall into the observed value ranges. When the absolute values between simulations and observations cannot be directly compared, the correlation coefficient (r) between original or transformed (e.g., logarithmic transformed) observations and simulations will be used. For example, the gene abundances from omics analysis cannot be directly compared to the enzyme concentrations or activities in the MEND model. However, we may assume correlation could be found between the measured and modeled values with a certain transformation or normalization. Noting that the coefficient of determination (R^2) is simply the square of the correlation coefficient (r) in case of a linear regression with an intercept. In other cases, e.g., a linear regression without including an intercept or a nonlinear fitting, R^2 may not be equivalent to r^2.

3.4. Model parameter calibration (optimization) algorithm

We use the modified Shuffled Complex Evolution (SCE) algorithm [69, 74, 75] to calibrate selected model parameters by minimize the overall objective function (J) as shown in Eq. S73a. SCE is a stochastic optimization method that includes competitive evolution of a 'complex' of points spanning the parameter space and the shuffling of complexes [69]. SCE has been widely used in calibration of hydrological, environmental, and ecosystem models and proved to be efficient and robust [1, 70, 76, 77, 78].

In this study, the multi-object weighted calibration was performed in two sequential steps. In the first step, ten microbial physiology parameters (r_E, p_{EP}, fp_{EM}; V_g, α, β, γ, K_D, Y_g; and r_0; see Table S5 for their definitions) were optimized using experimental observations of soil respiration (Rs), microbial biomass carbon (MBC), and soil organic carbon (SOC) (Table S7). We assigned weights of 0.5, 0.3, and 0.2 to Rs, MBC, and SOC, respectively, reflecting the substantially larger number of Rs measurements (32 data points) relative to MBC and SOC (2

observations each). In the second step, these calibrated microbial parameters were fixed, and five key inorganic N parameters (VN_{VG}, VN_{im}, VN_{fix}, VN_{nit}, and VN_{denit}; see Table S5 for their definitions) were optimized using observations of microbial C:N ratio, and concentrations of ammonium (NH_4^+) and nitrate (NO_3^-) (Table S7). In this stage, weights of 0.4, 0.3, and 0.3 were assigned to microbial C:N, NH_4^+, and NO_3^-, respectively. We further tested several alternative weighting schemes (W1–W3, Table S8). Across these schemes, the optimal parameter values and objective function values (Table S7) changed only modestly, indicating that the calibration is robust to reasonable variations in weighting (Table S8).

Supplementary Figures

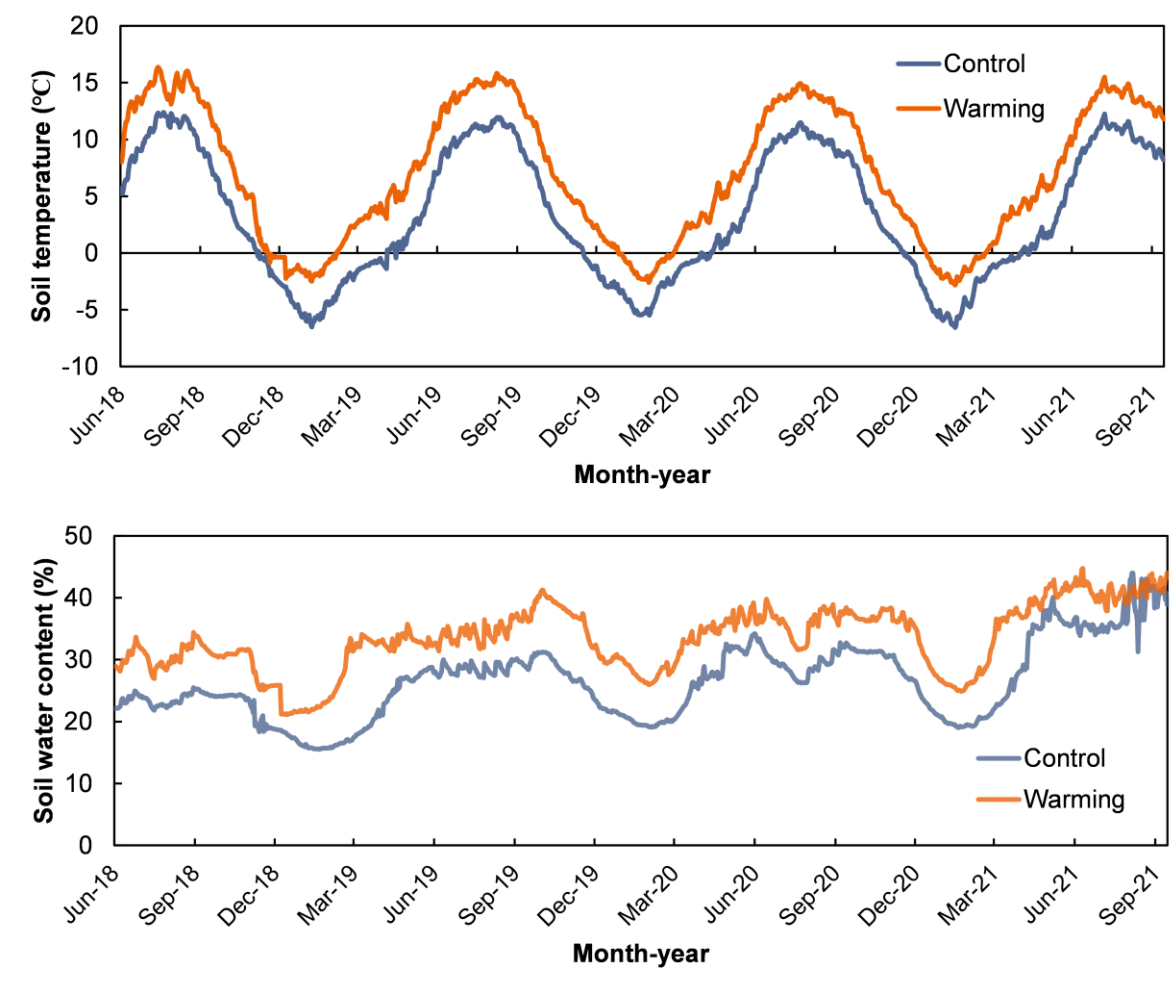

Fig. S2 | Mean soil temperature and soil water content (0–100 cm) observed under control and warming treatments.

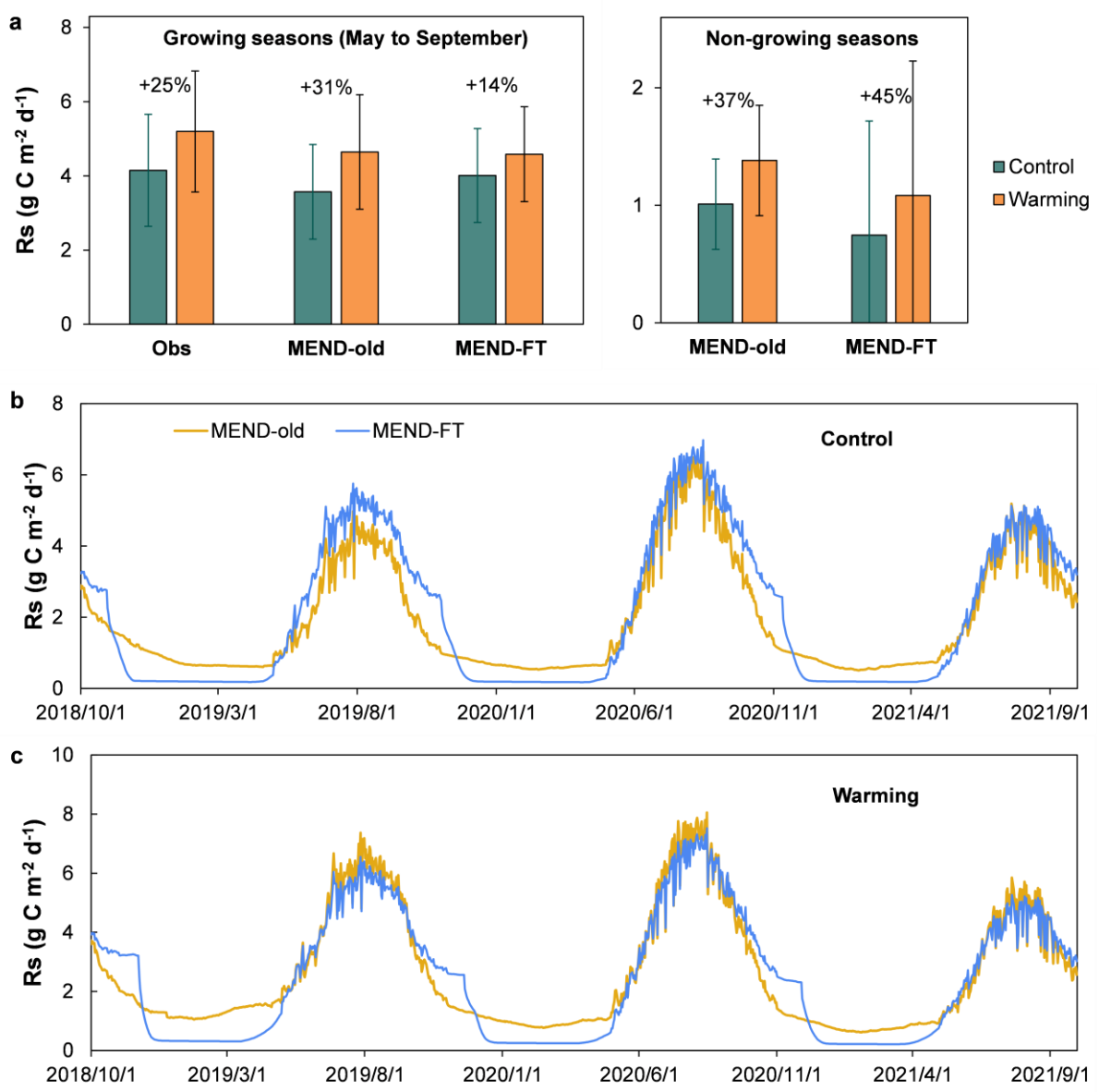

Fig. S3 | Soil respiration (Rs) responses to warming and continuous daily simulations. (a) Warming effects on Rs during the growing and non-growing seasons. Error bar denotes standard deviation. (b–c) Simulated daily Rs under control (b) and warming (c) treatments.

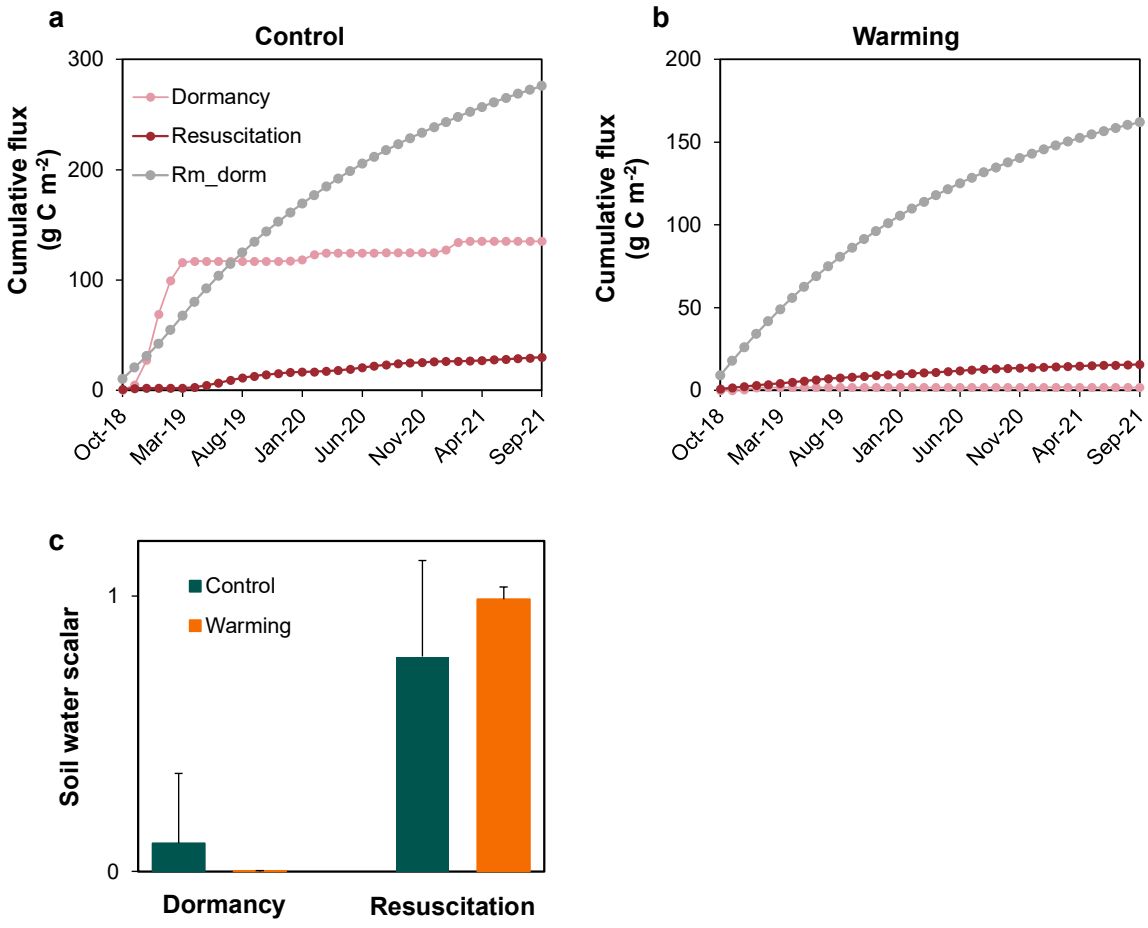

Fig. S4 | Microbial dormancy processes and soil water scalar in MEND-old. (a–b) Cumulative fluxes of dormancy, resuscitation, and dormant microbial maintenance respiration (Rm_dorm) under (a) control and (b) warming treatments. (c) Monthly mean soil water scalar regulating dormancy and resuscitation processes in MEND-old. Error bar means standard deviations (n = 36).

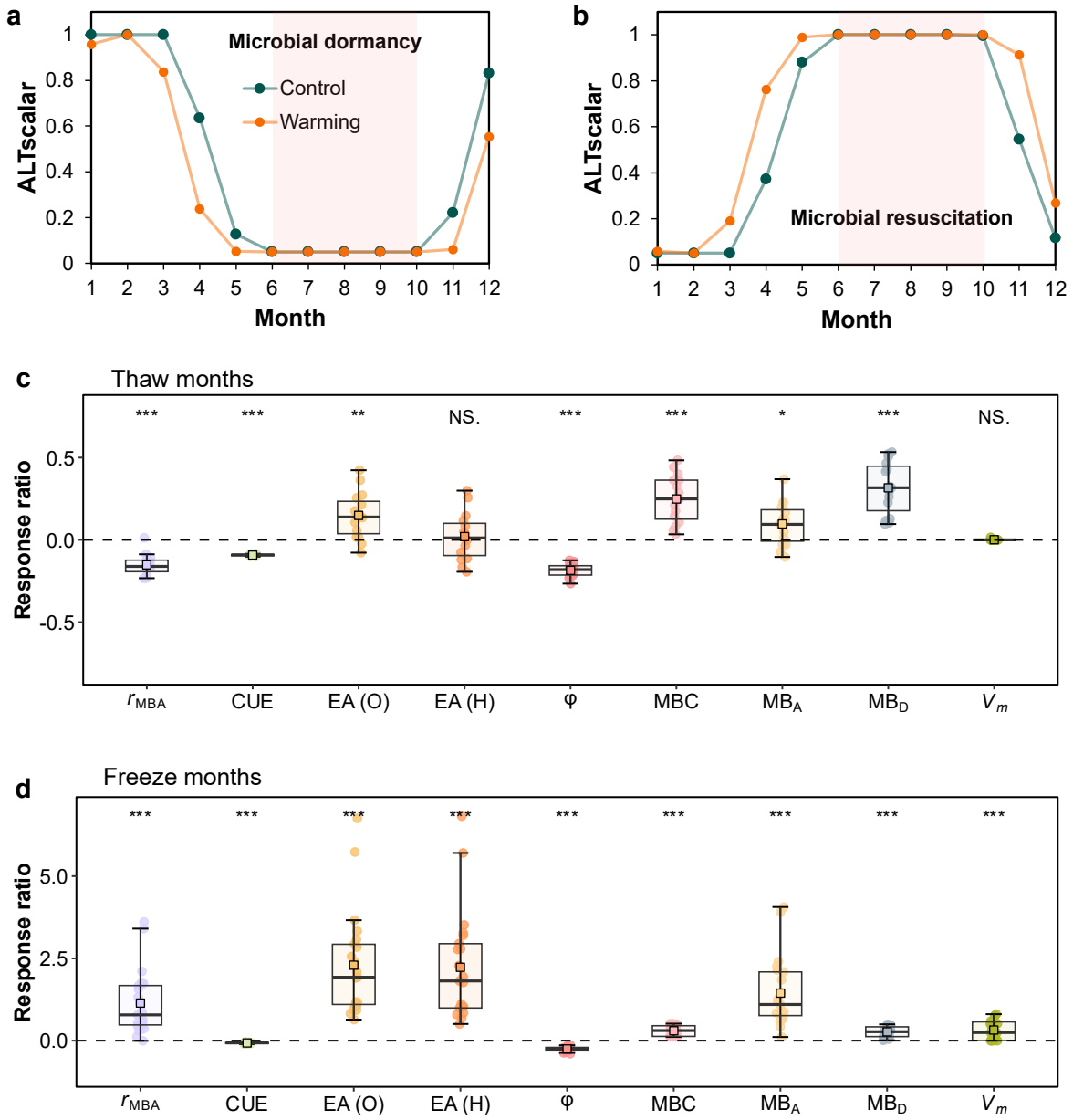

Fig. S5 | Freeze-thaw regulation (a–b) and simulated monthly microbial responses to warming across (c) all thaw-period months (June to October) and (d) freeze-period months (November to May). Variables include active fraction (r_{MBA}), microbial carbon use efficiency (CUE), enzyme activities (EA) of oxidases (O) and hydrolases (H), substrate availability (φ = DOM/(DOM + KsDOM)), microbial biomass carbon (MBC), active microbial biomass (MB_A) and dormant microbial biomass (MB_D), and biomass-specific maintenance rate (V_m). Differences between RR values and 0 were tested using the Wilcoxon test. "***" denotes a significance difference at $p < 0.01$; "NS." means not significant ($p > 0.05$).

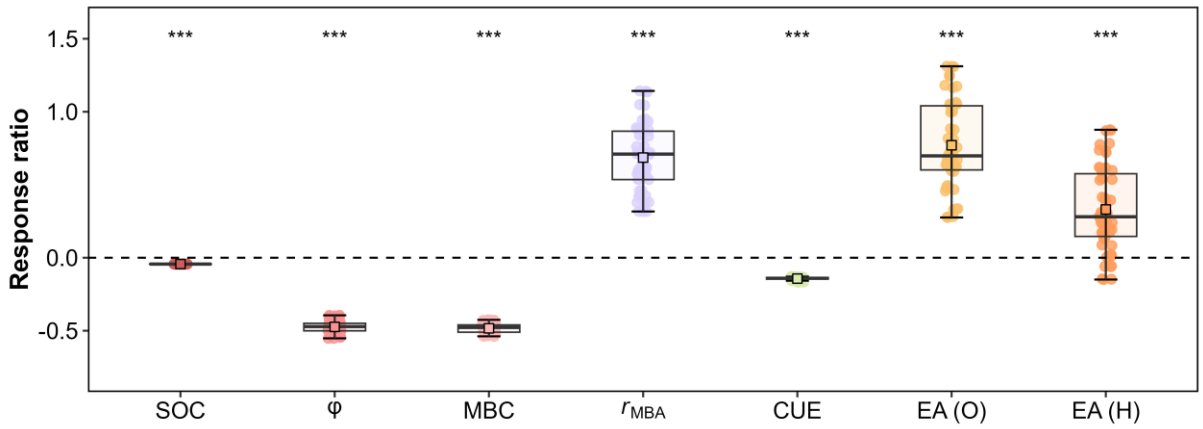

Fig. S6 | Long-term (50-year) warming effects on soil process and microbial activity simulated by MEND-old model. Soil variables include soil organic carbon (SOC), substrate availability (φ = DOM/(DOM + KsDOM)), and microbial biomass carbon (MBC). Microbial activity is expressed as active fraction (r_{MBA}), microbial carbon use efficiency (CUE), and enzyme activities (EA) of oxidases (O) and hydrolases (H). The dots represent yearly modeled values. Differences between RR values and 0 were tested using the Wilcoxon test. "***" denotes a significance difference at $p < 0.01$; "NS." means not significant ($p > 0.05$).

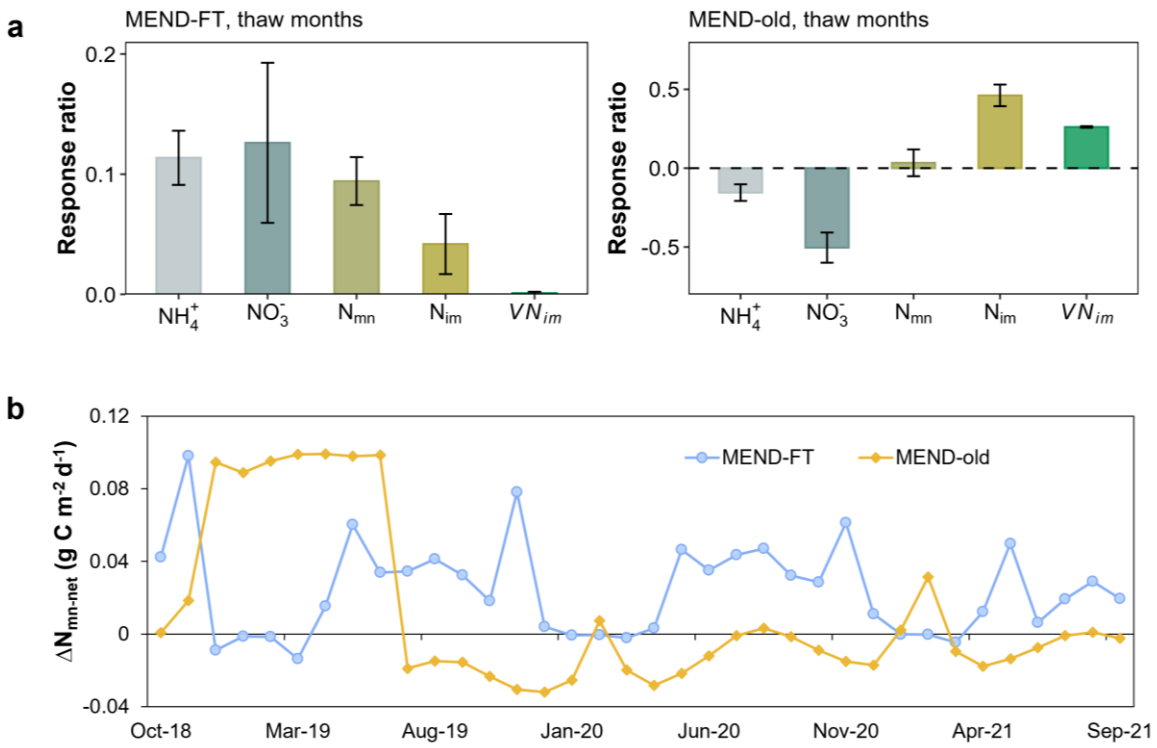

Fig. S7 | Simulated warming effects on inorganic N processes. (a) Response ratio (RR = $\ln(X_{Warming}/X_{Conrol})$) of NH_4^+ and NO_3^- pools, N mineralization (N_{mn}), N immobilization (N_{im}), and the maximum specific microbial N immobilization rate (VN_{im}) during thaw months (June to October) simulated by MEND-FT and MEND-old model. Error bar denotes standard error, n = 15. (b) Time series of warming-induced changes in net N mineralization flux ($N_{mn\text{-}net} = N_{mn} - N_{im}$), $\Delta N_{mn\text{-}net}$ denotes the difference of $N_{mn\text{-}net}$ between warming and control.

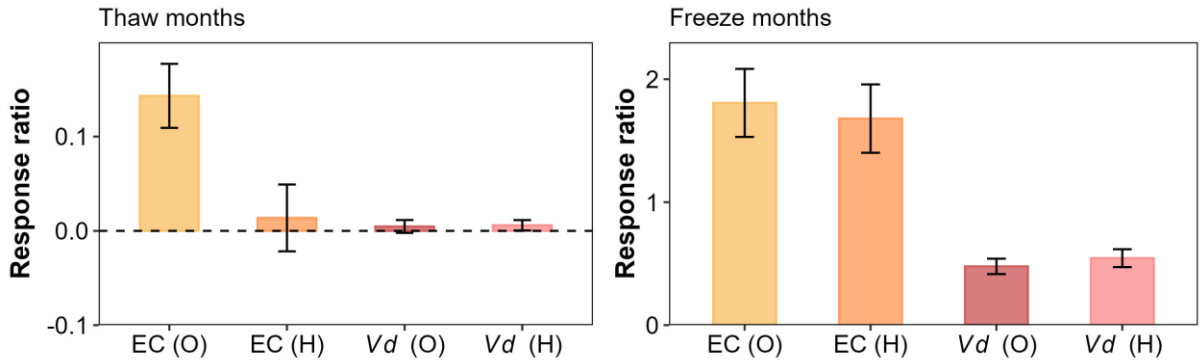

Fig. S8 | Simulated warming effects on enzyme concentration (EC) and specific enzyme activity (*Vd*). Response ratio (RR = $\ln(X_{Warming}/X_{Conrol})$) of EC and *Vd* of oxidases (O) and hydrolases (H) during thaw months (June to October) and freeze months (November to May) simulated by the MEND-FT. Error bar denotes standard error, n = 15.

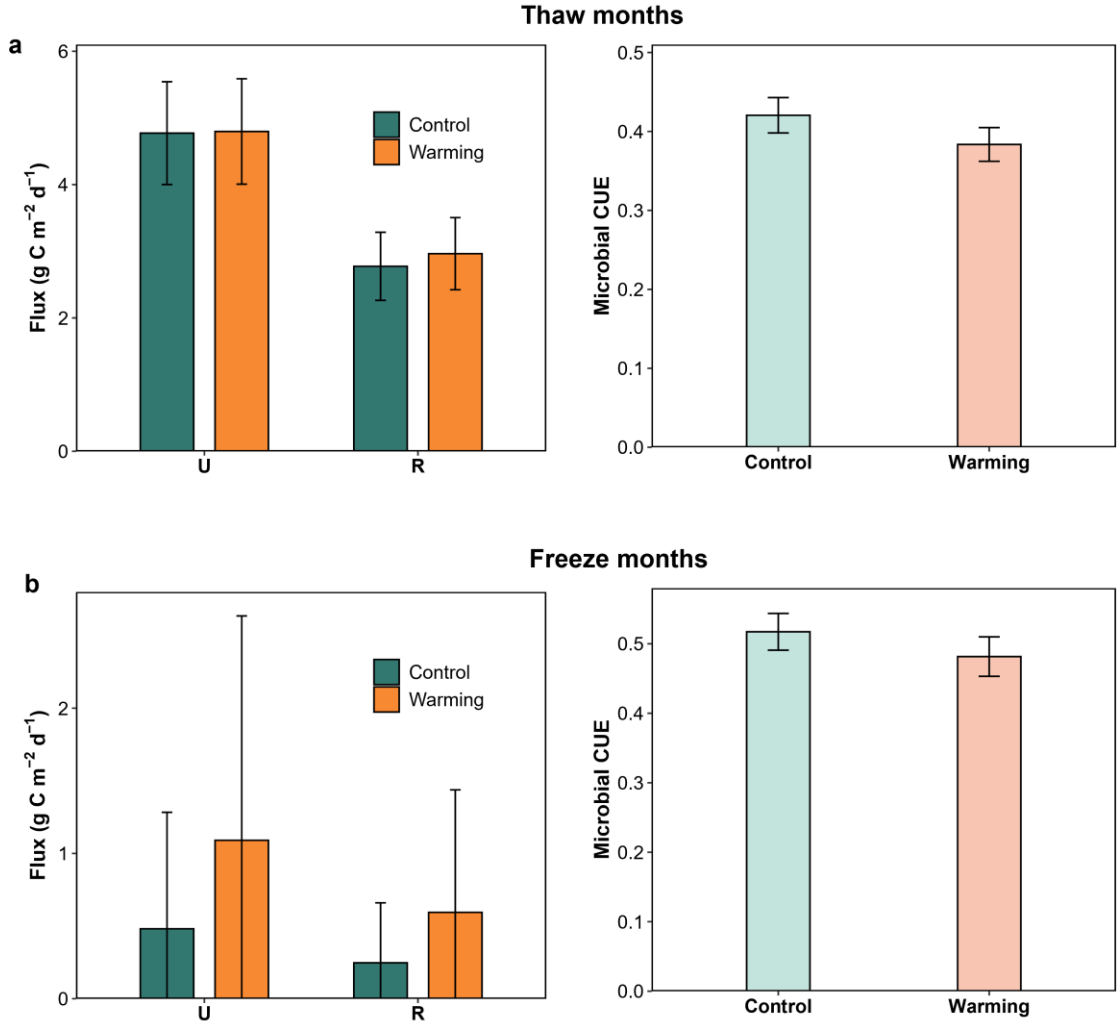

Fig. S9 | Seasonal microbial uptake, respiration and carbon use efficiency (CUE) simulated by the MEND-FT model. Shown are microbial uptake (U) and respiration (R) (left panels, mean ± s.d.), and CUE (right panels, mean ± s.d.) under control and warming treatments. Results are summarized for thaw months (June–October; n = 15) and freeze months (November–May; n = 21). Microbial CUE is calculated as (U − R)/U.

Supplementary Tables

Table S1. Soil carbon (C) and nitrogen (N) pools (state variables) in the MEND model

Soil C and/or N pool	**Pool name**	**Description** (*variable name*)
SOM pools	POM_O	Particulate organic matter (POM) decomposed by oxidative enzymes (*PO; PON*)
	POM_H	POM decomposed by hydrolytic enzymes (*PH; PHN*)
	MOM	Mineral-associated organic matter (*M; MN*)
	DOM	Dissolved organic matter (*D; DN*)
	QOM	Active MOM interacting with DOM (*Q; QN*)
SOM-degrading enzyme groups	EP_O	POM oxidative enzymes (*EPO; EPON*)
	EP_H	POM hydrolytic enzymes (*EPH; EPHN*)
	EM	MOM degrading enzymes (*EM; EMN*)
Inorganic-N enzyme groups	ENH4	Ammonium oxidases (*ENH4; ENH4N*)
	ENO3	Nitrate reductase (*ENO3*; *ENO3N*)
	ENO2	Nitrite reductases (*ENO2; ENO2N*)
	ENO	Nitric oxide reductases (*ENO; ENON*)
	EN2O	Nitrous oxide reductases (*EN2O; EN2ON*)
	EN2	Nitrogenases (*EN2; EN2N*)
Inorganic N pools	NH_4^+ Adsorb	Adsorbed ammonium (*NH4ads*)
	NH_4^+	Ammonium (*NH4*)
	NO_3^-	Nitrate (*NO3*)
	NO_2^-	Nitrite (*NO2*)
	NO	Nitric oxide (*NO*)
	N_2O	Nitrous oxide (*N2O*)
	N_2	Dinitrogen (*N2*)
Microbial functional groups	MB_A	Active microbial biomass (*BA; BAN*)
	MB_D	Dormant microbial biomass (*BD; BDN*)

Table S2. Governing equations for each soil C or N pool (Table S1) in the MEND model

Governing Equation	**Eq#**
Soil Carbon	
$dPO/dt = I_{PO} + (1 - g_D) \cdot g_{PO} \cdot F_9 - F_1$; $I_{PO} + I_{PH} + I_D = I_{gross} \cdot fINP$; I_{gross} is gross litter input	(S1)
$dPH/dt = I_{PH} + (1 - g_D) \cdot (1 - g_{PO}) \cdot F_9 - F_2$	(S2)
$dM/dt = (1 - f_D) \cdot (F_1 + F_2) - F_3$	(S3)
$dQ/dt = F_4 - F_5$	(S4)
$dD/dt = I_D + f_D \cdot (F_1 + F_2) + F_3 + g_D \cdot F_9 + F_{16} - F_6 - (F_4 - F_5)$	(S5)
$dBA/dt = F_6 - (F_7 - F_8) - F_9 - (F_{10} + F_{11} + F_{12}) - (F_{15} + F_{17}) + F_{18}$	(S6)
$dBD/dt = (F_7 - F_8) - (F_{13} + F_{14})$	(S7)
$dED_i/dt = F_{15,ED_i} - F_{16,ED_i}$; ED_i $(i = 1,2,3)$ denotes *EPO*, *EPH*, *EM*, respectively	(S8)
$dEN_j/dt = F_{17,EN_j} - F_{18,EN_j}$; EN_j $(j = 1,2,\cdots,6)$ denotes *ENH4*, *ENO3*, *ENO2*, *ENO*, *EN2O*, *EN2*, respectively	(S9)
$R_h = (F_{10} + F_{11} + F_{12}) + (F_{13} + F_{14})$; heterotrophic (microbial) respiration	(S10)
$R_a = fR_a \cdot GPP$; autotrophic (root) respiration	(S11)
$R_s = R_a + R_h$; total soil respiration	(S12)
$\frac{d}{dt}\left(PO + PH + M + Q + D + BA + BD + \sum_{i=1}^{3} ED_i + \sum_{j=1}^{6} EN_i\right) = (I_{PO} + I_{PH} + I_D) - R_h$	(S13)
Soil Nitrogen	
• For soil organic matter pools, the *N* flux: $FN_k = F_k / CN_{source}$, where F_k (k = 1–9) is the *C* flux, and CN_{source} is the C:N ratio of the (upstream) source pool.	(S14a)
• For enzymes pools ED_i (i=1,2,3) and EN_j (j=1…6), the *N* flux $FN_k = F_k / CN_{ENZ}$, k = 15–18.	(S14b)
$\frac{dBAN}{dt} = \frac{F_6}{CN_D} - \left(\frac{F_7}{CN_{BA}} - \frac{F_8}{CN_{BD}}\right) - \frac{F_9}{CN_{BA}} - \frac{F_{15}+F_{17}}{CN_{ENZ}} + \frac{F_{18}}{CN_{ENZ}} - FN_{mn,BA} + \left(FN_{im,NH4\to BA} + FN_{im,NO3\to BA}\right)$	(S15)
$dBDN/dt = (F_7/CN_{BA} - F_8/CN_{BD}) - FN_{mn,BD}$	(S16)
$dNH4/dt = I_{NH4} + FN_{fix} + \left(FN_{mn,BA} + FN_{mn,BD}\right) - \left(FN_{im,NH4\to BA} + FN_{im,NH4\to VG}\right) - FN_{nit}$	(S17)
$dNO3/dt = I_{NO3} + FN_{nit} - FN_{nit-denit} - FN_{denit_2} - \left(FN_{im,NO3\to BA} + FN_{im,NO3\to VG}\right) - FN_{leach,NO3}$	(S18)
$dNO2/dt = FN_{denit_2} - FN_{denit_3} - FN_{leach,NO2}$	(S19)
$dNO/dt = FN_{denit_3} - FN_{denit_4} - FN_{emit_4}$	(S20)
$dN2O/dt = FN_{nit-denit} + FN_{denit_4} - FN_{denit_5} - FN_{emit_5}$	(S21)
$dN2/dt = FN_{denit_5} - FN_{fix} - FN_{emit_6}$	(S22)
$\frac{d}{dt}\left(PON + PHN + MN + QN + DN + BAN + BDN + \sum_{i=1}^{3} EDN_i + \sum_{j=1}^{6} ENN_i\right) = (IN_{PO} + IN_{PH} + IN_D) + \left(FN_{im,NH4\to BA} + FN_{im,NO3\to BA}\right) - \left(FN_{mn,BA} + FN_{mn,BD}\right)$	(S23a)
$\frac{d}{dt}\left(NH4ads + \sum_{j=1}^{6} N_j\right) = (I_{NH4} + I_{NO3}) + \left(FN_{mn,BA} + FN_{mn,BD}\right) - \left(FN_{im,NH4\to BA} + FN_{im,NO3\to BA}\right) - \left(FN_{im,NH4\to VG} + FN_{im,NO3\to VG}\right) - \left(FN_{leach,NO3} + FN_{leach,NO2}\right) - \sum_{j=4}^{6} NF_{emit_j}$	(S23b)
$\frac{d}{dt}\left(PON + PHN + MN + QN + DN + BAN + BDN + \sum_{i=1}^{3} EDN_i + \sum_{j=1}^{6} ENN_i + \sum_{j=1}^{6} N_j + NH4ads\right) = (IN_{PO} + IN_{PH} + IN_D) + (I_{NH4} + I_{NO3}) - \left(FN_{im,NH4\to VG} + FN_{im,NO3\to VG}\right) - \left(FN_{leach,NO3} + FN_{leach,NO2}\right) - \sum_{j=4}^{6} NF_{emit_j}$	(S23c)

Table S3. Component fluxes in the MEND model (parameters are shown in Table S5)

Flux description	**Equation**	**Eq#**
Particulate organic matter (POM) pool (oxidative) (*PO*) decomposition (F_1)	$F_1 = Vd_{PO} \cdot EPO \cdot PO/(K_{PO} + PO)$	(S24)
POM pool (hydrolytic) (*PH*) decomposition	$F_2 = Vd_{PH} \cdot EPH \cdot PH/(K_{PH} + PH)$	(S25)
Mineral-associated organic matter (*M*) decomposition	$F_3 = Vd_M \cdot EM \cdot M/(K_M + M)$	(S26)
Adsorption (F_4) and desorption (F_5) between dissolved organic matter (*D*) and adsorbed DOM (*Q*)	$F_4 = k_{ads} \cdot (1 - Q/Q_{max}) \cdot D$ $F_5 = k_{des} \cdot (Q/Q_{max})$ $K_{ads} = K_{des} \cdot K_{ba}$	(S27) (S28)
DOM (*D*) uptake by microbes	$F_6 = \frac{1}{Y_g}(V_g + V_m) \cdot \frac{BA \cdot D}{K_D + D}$	(S29)
Dormancy (F_7) and resuscitation (F_8) between active (*BA*) and dormant (*BD*) microbes	$F_7 = [1 - D/(K_D + D)] \cdot V_m \cdot BA$ $F_8 = [D/(K_D + D)] \cdot V_m \cdot BD$	(S30) (S31)
MB_A (*BA*) mortality	$F_9 = \gamma \cdot V_m \cdot BA$	(S32)
MB_A (*BA*) growth respiration (F_{10}) and maintenance respiration (F_{11})	$F_{10} = \left(\frac{1}{Y_g} - 1\right) \cdot \frac{V_g \cdot BA \cdot D}{K_D + D}$ $F_{11} = \left(\frac{1}{Y_g} - 1\right) \cdot \frac{V_m \cdot BA \cdot D}{K_D + D}$	(S33) (S34)
MB_A (*BA*) overflow respiration (F_{12})	$F_{12} = max\{0, BA - BAN \cdot CN_{BA,max}\}$	(S35)
MB_D (*BD*) maintenance respiration (F_{13})	$F_{13} = \beta \cdot V_m \cdot BD$	(S36)
MB_D (*BD*) overflow respiration (F_{14})	$F_{14} = max\{0, BD - BDN \cdot CN_{BA,max}\}$	(S37)
Synthesis of enzymes for decomposition of *PO* ($F_{15,EPO}$, $EPO = ED_1$), *PH* ($F_{15,EPH}$, $EPH = ED_2$), and *M* ($F_{15,EM}$, $EM = ED_3$)	$F_{15,EPO} = PO/(PO + PH) \cdot p_{EP} \cdot V_m \cdot BA$ $F_{15,EPH} = PH/(PO + PH) \cdot p_{EP} \cdot V_m \cdot BA$ $F_{15,EM} = fp_{EM} \cdot p_{EP} \cdot V_m \cdot BA$ $F_{15} = \sum_{i=1}^{3} F_{15,ED_j} = F_{15,EPO} + F_{15,EPH} + F_{15,EM}$	(S38)
Turnover of enzymes ($EPO = ED_1$, $EPH = ED_2$, $EM = ED_3$)	$F_{16,ED_i} = r_E \cdot ED_i$ $F_{16} = \sum_{i=1}^{3} F_{16,ED_j}$	(S39)
Synthesis of enzyme groups for inorganic-N transformations; EN_j ($j = 1 - 6$): *ENH4*, *ENO3*, *ENO2*, *ENO*, *EN2O*, *EN2*; SON_i ($i = 1 - 5$): *PON*, *PHN*, *MN*, *QN*, *DN*	$F_{17} = \sum_{j=1}^{6} F_{17,EN_j} = F_{15} \cdot (NH4 + NO3 + NO2)/\sum_{i=1}^{4} SON_i$ $F_{17,EN_j} = \frac{N_j/KSN_j}{\sum_{j=1}^{6}(N_j/KSN_j)} \cdot F_{17}$	(S40)
Turnover of enzymes for nitrification, denitrification, and N fixation	$F_{18} = \sum_{j=1}^{6} F_{18,EN_j}$; $F_{18,EN_j} = r_E \cdot EN_j$	(S41)

Table S4. Inorganic N fluxes in the MEND model (parameters are shown in Table S5)

Flux description	Equation	Eq#
Nitrification	$FN_{nit} = \frac{VN_{nit} \cdot ENH4 \cdot NH4}{KSN_1 + NH4}$	(S42)
Nitrifier Denitrification	$FN_{nit-denit} = FN_{nit} \cdot [1 - f(O_2)]$	(S43a)
	$f(O_2) = \frac{(1-WFP)^{4/3}}{0.5^{4/3} + (1-WFP)^{4/3}}$; *WFP* is water-filled porosity	(S43b)
Denitrification of *NO3*, *NO2*, *NO*, *N2O*: j = 2, 3, 4, 5	$FN_{denit_j} = \frac{VN_j \cdot EN_j \cdot N_j}{KSN_j + N_j}$	(S44)
N fixation	$FN_{fix} = \frac{VN_{fix} \cdot EN2 \cdot N2}{KSN_6 + N2} \cdot \left(1 - \frac{NH4}{KSN_1 + NH4}\right)$	(S45)
N mineralization	$FN_{mn,BA} = (1 - YN_g) \cdot FN_6$	(S46)
	$YN_g = \left(\frac{CN_{BA} - CN_{BA,min}}{CN_{BA,max} - CN_{BA,min}}\right)^{\omega}$	(S47)
N immobilization by microbes	$FN_{im,NH4 \to BA} = \left[(VN_{im,NH4} \cdot YN_g) \cdot BA \cdot NH4\right] / (KSN_{BA1} \cdot \eta)$	(S48)
	$FN_{im,NO3 \to BA} = \left[(VN_{im,NO3} \cdot YN_g) \cdot BA \cdot NO3\right] / (KSN_{BA2} \cdot \eta)$	(S49)
	$\eta = 1 + \frac{BA}{KSN_{BA1}} + \frac{NH4}{KSN_{BA1}} + \frac{NO3}{KSN_{BA2}} + \frac{NH4}{KSN_{VG1}} + \frac{NO3}{KSN_{VG2}}$	(S50)
N uptake by plants	$FN_{im,NH4 \to VG} = \left[(VN_{VG,NH4} \cdot rGPP) \cdot NH4\right] / (KSN_{VG1} \cdot \eta)$	(S51)
	$FN_{im,NO3 \to VG} = \left[(VN_{VG,NO3} \cdot rGPP) \cdot NO3\right] / (KSN_{VG2} \cdot \eta)$	(S52)
	Coefficient *rGPP* =*f*(GPP), e.g., $rGPP = \exp[\omega_{VG} \cdot (GPP/GPP_{ref} - 1)]$	
NH_4^+ sorption	$NH4 = \left[A + \sqrt{A^2 + 4K_{ba,NH4} \cdot NH4tot}\right] / (2 \cdot K_{ba,NH4})$	(S53a)
	$NH4ads = NH4tot - NH4$	(S53b)
	where $A = K_{ba,NH4} \cdot (NH4tot - NH4_{max}) - 1$	(S53c)
	derived from: $NH4ads + NH4 = NH4tot$	(S53d)
	$NH4ads = NH4_{max} \cdot (K_{ba,NH4} \cdot NH4) / (1 + K_{ba,NH4} \cdot NH4)$	(S53e)
NO_3^- and NO_2^- leaching	$FN_{leach,NO3} = NO3 \cdot fN_{leach}$	(S54a)
	$FN_{leach,NO2} = NO2 \cdot fN_{leach}$	(S54b)
	where: $fN_{leach} = r_{leach} \cdot fN_{dissolved} \cdot (\theta_{perc}/\theta)$	(S54c)
	$fN_{dissolved} = (\theta/\theta_{sat})^3$	(S54d)
	$\theta_{perc} = \theta_{excess} \cdot [1 - \exp(-\Delta t/TT_{perc})]$	(S54e)
	$\theta_{excess} = \max(0, \theta - \theta_{FC})$	(S54f)
	$TT_{perc} = (\theta_{sat} - \theta_{FC}) \cdot Depth/K_{sat}$	(S54g)
	$r_{leach} \in (0,1)$: scaling factor;	
	θ: volumetric soil water content (SWC); θ_{sat} and θ_{FC}: SWC at saturation and field capacity; *Depth*: soil depth (cm); θ_{excess}: excess SWC available for percolation; θ_{perc}: SWC percolation; K_{sat}: saturated hydraulic conductivity (cm h^{-1}); Δt: given time-period (= 1h); TT_{perc}: travel time for percolation (h)	
NO, N_2O, N_2 gas emission: j = 4,5,6	$FN_{emit_j} = [Ds_j \cdot (N_j - Nair_j)/(0.5 \cdot Depth)]/Depth$	(S55)
	where: Ds_j: gas diffusivity in soil (cm^2 h^{-1});	
	N_j and $Nair_j$ gas concentration in soil and air (mg N cm^{-3})	

Table S5. MEND model parameters

ID	Parameter	Description	Range	Value	Units
1	LF_0	Initial fraction of *PO*, $LF_0 = PO/(PO+PH)$	(0.1, 1.0)	0.61	—
2	$\boldsymbol{r_0}$	Initial active fraction of microbes	(0.01, 1)	**Calibrated**	—
3	fR_a	Scaling factor for autotrophic respiration (R_a)	(0.1, 0.4)	0.2	—
4	*fINP*	Scaling factor for litter input rate	(0.1, 0.9)	0.4	—
5	*VP*	Maximum specific decomposition rate	(0.1, 100)	20	mg C mg^{-1} C h^{-1}
6	K_{PO}	Half-saturation constant (HSC) for *PO* decomposition	(40,100)	60	mg C cm^{-3} soil
7	fK_M	$K_M = K_{PO} \times fK_M$, $K_{PH} = K_{PO}/fK_M$ K_{PH} and K_M are HSC for *PH* and *M*, respectively	(2, 20)	10	—
8	Q_{max}	Maximum sorption capacity	(0.5, 5.0)	3.6	mg C cm^{-3} soil
9	K_{ba}	Binding affinity	(1, 16)	8.7	(mg C cm^{-3} soil) $^{-1}$
10	k_{des}	Desorption rate for DOM	(1e-4, 0.01)	0.0053	mg C cm^{-3} soil h^{-1}
11	$\boldsymbol{r_E}$	Enzyme turnover rate	(1e-4, 0.01)	**Calibrated**	mg C mg^{-1} C h^{-1}
12	$\boldsymbol{p_{EP}}$	$[V_m \times p_{EP}]$ is the production rate of *EP* (*EPO* + *EPH*), V_m is the specific maintenance rate for *BA*	(1e-3, 0.1)	**Calibrated**	—
13	$\boldsymbol{fp_{EM}}$	$fp_{EM} = p_{EM}/p_{EP}$, $[V_{mt} \times p_{EM}]$ is the production rate of *EM*	(0.1, 5.0)	**Calibrated**	—
14	f_D	Fraction of decomposed *PO* and *PH* allocated to *D*	(0.05, 1)	0.8	—
15	g_D	Fraction of dead *BA* allocated to *D*	(0.01, 1)	0.4	—
16	g_{PO}	$(1 - g_D) \cdot g_{PO}$ is the fraction of dead *BA* entering *PO*	(0.05, 0.2)	0.1	—
17	$\boldsymbol{V_g}$	Maximum specific uptake rate of *D* for growth	(1e-3, 0.1)	**Calibrated**	mg C mg^{-1} C h^{-1}
18	$\boldsymbol{\alpha}$	$= V_m / (V_g + V_m)$, V_m is max specific maintenance rate	(0.01, 0.5)	**Calibrated**	—
19	K_D	HSC for microbial uptake of *D*	(1e-4, 0.5)	0.26	mg C cm^{-3} soil
20	$\boldsymbol{Y_g(T_{ref})}$	Intrinsic C use efficiency at reference temperature (T_{ref})	(0.2, 0.4)	**Calibrated**	—
21	kY_g	Slope for Y_g dependence of temperature	(1e-3, 0.016)	0.01	1/°C
22	Q_{10}	Q_{10} for temperature response function	(1.2, 2.5)	1.8	—
23	$\boldsymbol{\gamma}$	Max microbial mortality rate = $V_m \times \gamma$	(0.01, 20)	**Calibrated**	—
24	$\boldsymbol{\beta}$	Ratio of dormant maintenance rate to V_m	(5e-4, 0.05)	**Calibrated**	—
25	ψ_{A2D}	Soil water potential (SWP) threshold for microbial dormancy; both ψ_{A2D} & $\psi_{D2A} < 0$	(–0.6, –0.2)	0.46	MPa
26	τ	$\psi_{D2A} = \psi_{A2D} \times \tau$, ψ_{D2A} is the SWP threshold for microbial resuscitation	(0.1, 0.9)	0.39	—
27	ω	Exponential in SWP function for microbial dormancy or resuscitation	(1, 6)	3.38	—

28	*ALTa*	Shape parameter for available substrate distribution (*a* in Eq. S60, Table S6)	(0.1, 2)	0.54	—
29	*ALTb*	Shape parameter for microbial dormancy and resuscitation (*b* in Eqs. S61 and S62, TableS6)	(0.1, 2)	0.6	—
30	*ALTc*	The minimal dormancy and resuscitations response values (f_{A2D}(ALTscalar)_min and f_{D2A}(ALTscalar)_min)	(0.01, 0.2)	0.05	—
Inorganic nitrogen parameters					
31	$\boldsymbol{VN_{im,BA}}$	Max specific microbial N immobilization rate	(1e-4, 0.1)	**Calibrated**	mg N mg^{-1} C h^{-1}
32	KSN_{BA1}	HSC for microbial immobilization of NH_4^+	(1e-4, 0.01)	1.8e-4	mg N cm^{-3} soil
33	KSN_{BA2}	HSC for microbial immobilization of NO_3^-	(1e-4, 0.01)	4.1e-4	mg N cm^{-3} soil
34	$\boldsymbol{VNit}$	Max specific nitrification rate (VN_1)	(0.1, 1000)	**Calibrated**	mg N mg^{-1} C h^{-1}
35	$\boldsymbol{VN_{denit}}$	Max specific denitrification rate	(1e-4, 1.0)	**Calibrated**	mg N mg^{-1} C h^{-1}
36	$\boldsymbol{VNif}$	Max specific N fixation rate (VN_6)	(1e-4, 0.1)	**Calibrated**	mg N mg^{-1} C h^{-1}
37	KSN_1	HSC for nitrification	(1e-3, 1.0)	0.0012	mg N cm^{-3} soil
38	KSN_2	HSC for denitrification of NO_3^- and NO_2^-	(1e-4, 0.1)	0.0018	mg N cm^{-3} soil
39	KSN_4	HSC for denitrification of NO and N_2O	(1e-4, 0.1)	0.0018	mg N cm^{-3} soil
40	KSN_6	HSC for N fixation	(1e-4, 0.1)	0.1	mg N cm^{-3} soil
41	$\boldsymbol{VN_{VG}}$	Max plant N uptake rate	(1e-6, 1e-3)	**Calibrated**	mg N cm^{-3} h^{-1}
42	KSN_{VG1}	HSC for plant uptake of NH_4^+	(1e-4, 0.01)	0.0012	mg N cm^{-3} soil
43	KSN_{VG2}	HSC for plant uptake of NO_3^-	(1e-4, 0.01)	0.0018	mg N cm^{-3} soil
44	ω_{VG}	Exponential for calculating *rGPP* as a function of GPP	(0.01, 1)	0.5	—
45	$NH4_{max}$	Maximum sorption capacity for NH_4^+	(1e-5, 0.01)	0.0057	mg N cm^{-3} soil
46	$K_{ba,NH4}$	Binding affinity for NH_4^+	(1, 1e4)	100	(mg N cm^{-3} soil)$^{-1}$
47	r_{leach}	Scaling factor for NO_3^- and NO_2^- leaching	(0.01, 1)	0.02	—

Table S6. MEND model response functions

Function description	Response function	Variables and Parameters	Eq#
Reaction rate (MEND-old)	$v = v_0 \cdot f(\psi) \cdot f(T) \cdot f(pH)$ $f(\psi)$: soil moisture response function (SMRF) $f(T)$: soil temperature response function; $f(pH)$: pH response function	v_0: baseline reaction rate; ψ: soil water potential, SWP (MPa); *T*: soil temperature; *pH*: soil pH	(S56)
Reaction rate (MEND-FT)	$v = v_0 \cdot f(\psi) \cdot f(\text{ALTscalar}) \cdot f(pH)$ $f(\text{ALTscalar})$: freeze-thaw (FT) response function;	ALTscalar is the relative thawed proportion, calculated based on frozen depth (*zFrozen*, cm), thawed depth (*zThaw*, cm), and total soil depth (*zSoil*, cm), see Eq. S59.	(S57)
Dormancy and resuscitation rate (MEND-FT)	$v = v_0 \cdot f(\text{ALTscalar})$		(S58)
ALTscalar in seasonally frozen soils	$\text{ALTscalar} = \begin{cases} 1, & zFrozen = 0 \\ \min\left(\frac{\max(zThaw, zThaw+zSoil-zFrozen)}{zSoil}, 1\right), & zFrozen > 0 \text{ and } zThaw > 0 \\ \max\left(1-\frac{zFrozen}{zSoil}, 0\right), & zFrozen > 0 \text{ and } zThaw = 0 \end{cases}$		(S59a)
ALTscalar in permafrost regions	$\text{ALTscalar} = \begin{cases} 0, & zThaw = 0 \\ \min\left(\frac{zThaw}{zSoil}, 1\right), & zThaw > 0 \text{ and } zFrozen = 0 \\ \max\left(1-\frac{zFrozen}{zSoil}, 0\right), & zFrozen > 0 \text{ and } zThaw > 0 \end{cases}$		(S59b)
Freeze-thaw response function for decomposition.	$f_{\text{dec}}(\text{ALTscalar}) = \begin{cases} 1, & \text{whole soil thawed} \\ f_{dec}(\text{ALTscalar})\_\text{min}, & \text{whole soil frozen} \\ \frac{(1+a)\cdot\text{ALTscalar}}{a+\text{ALTscalar}}, & \text{soil thawing} \\ 1-\frac{(1+a)(1-\text{ALTscalar})}{a+(1-\text{ALTscalar})}, & \text{soil freezing} \end{cases}$	*a*: model parameter *ALTa* in Table S5 shapes available substrate distribution. the minimal function value (f_{dec}(ALTscalar_min)), which is depending on site-specific distribution of substrate in the soil profile.	(S60)
FT response function for dormancy	$f_{\text{A2D}}(\text{ALTscalar}) = \begin{cases} f_{\text{A2D}}(\text{ALTscalar})\_\text{min}, & \text{whole soil thawed} \\ 1, & \text{whole soil frozen} \\ \frac{b(1-\text{ALTscalar})}{b+\text{ALTscalar}}, & \text{soil thawing} \\ 1-\frac{b\cdot\text{ALTscalar}}{b+(1-\text{ALTscalar})}, & \text{soil freezing} \end{cases}$	*b*: model parameter *ALTb* in Table S5, shapes the corresponding function, $b = 1.11a$. The minimal function value (f_{A2D}(ALTscalar)_min) is parameter *ALTc* in Table S5.	(S61)
FT response function for resuscitation	$f_{\text{D2A}}(\text{ALTscalar}) = \begin{cases} 1, & \text{whole soil thawed} \\ f_{\text{D2A}}(\text{ALTscalar})\_\text{min}, & \text{whole soil frozen} \\ \frac{(1+b)\cdot\text{ALTscalar}}{b+\text{ALTscalar}}, & \text{soil thawing} \\ 1-\frac{(1+b)(1-\text{ALTscalar})}{b+(1-\text{ALTscalar})}, & \text{soil freezing} \end{cases}$	*b*: model parameter *ALTb* in Table S5, shapes the corresponding function, $b = 1.11a$. The minimal function value (f_{D2A}(ALTscalar)_min) is parameter *ALTc* in Table S5.	(S62)
Soil pH response function	$f(pH) = exp\left[-\left(\frac{pH-pH_{opt}}{pH_{sen}}\right)^2\right]$	pH_{opt}: optimum *pH* that gives the maximum reaction rate; pH_{sen}: sensitivity of the reaction rate to deviation from pH_{opt}	(S63)
Temperature sensitivity of	$Y_g(T) = Y_g(T_{ref}) - k_{Yg}\cdot(T-T_{ref})$	$Y_g(T_{ref})$: Y_g at reference temperature, T_{ref} (°C);	(S64)

intrinsic carbon use efficiency (Y_g)		$-k_{Yg}$: the slope, –0.016 ≤ $-k_{Yg}$ ≤ –0.001 °C $^{-1}$	
Temperature response: Arrhenius equation or Q_{10} method	$f(T) = exp\left[-\frac{Ea}{R}\left(\frac{1}{T}-\frac{1}{T_{ref}}\right)\right]$ $f(T) = Q_{10}^{\frac{T-T_{ref}}{10}}$ $Q_{10} = exp\left[\frac{Ea}{R \cdot T_{ref}} \cdot \frac{10}{T}\right]$	T: temperature (K); T_{ref}: reference temperature (K); Ea: activation energy (kJ mol^{-1}); R = 8.314 J mol^{-1} K^{-1}, the universal gas constant; Q_{10}: the factor by which the reaction rate is multiplied when temperature increases over T_{ref} by 10 K	(S65) (S66) (S67)
SMRF for SOM decomposition by oxidative enzymes	$f_{oxi}(\psi) = \begin{cases} 0, & \psi \le -10^{2.5} \\ 0.625 - 0.25 \times \log_{10}(-\psi), & -10^{2.5} < \psi \le -10^{1.5} \\ 1, & -10^{1.5} < \psi \le -10^{-2.5} \\ [2.5 + 0.4 \times \log_{10}(-\psi)]/1.5, & -10^{-2.5} < \psi \le -10^{-4} \\ 0.6, & \psi > -10^{-4} \end{cases}$	ψ: soil water potential (MPa) Hansen et al. [55]	(S68)
SMRF for SOM decomposition by hydrolytic enzymes	$f_{hyd}(\psi) = \begin{cases} 0, & \psi \le \psi_{min} \\ 1 - \left[\frac{\ln(\psi/\psi_{FC})}{\ln(\psi_{min}/\psi_{FC})}\right]^b, & \psi_{min} < \psi \le \psi_{FC} \\ 1, & \psi > \psi_{FC} \end{cases}$	ψ: soil water potential (MPa); ψ_{FC}= −0.033 MPa: SWP at field capacity; ψ_{min}: microbial stress threshold SWP; b: a shape parameter Manzoni *et al.* [56]	(S69)
SMRF for microbial dormancy & resuscitation	$f_{A2D}(\psi) = \frac{1}{1 + [\psi_{A2D}/\psi]^\omega}$ $f_{D2A}(\psi) = \frac{1}{1 + (\psi/\psi_{D2A})^\omega} = \frac{1}{1 + [\psi/(\psi_{A2D} \times \tau)]^\omega}$	ψ_{A2D} (MPa): critical SWP for microbial dormancy; ψ_{D2A} (MPa): critical SWP for microbial resuscitation; $\tau = \psi_{D2A}/\psi_{A2D}$; ω: exponent to describe the steepness of the curve	(S70) (S71)
SMRF for nitrification & denitrification	$f(WFP) = \begin{cases} 0 & WFP \le WFP_1 \\ a_+ + b_+ \cdot WFP & WFP_1 < WFP \le WFP_2 \\ 1 & WFP_2 < WFP \le WFP_3 \\ a_- + b_- \cdot WFP & WFP_3 < WFP \le WFP_4 \\ 0 & WFP > WFP_4 \end{cases}$	$WFP = \theta/\phi$: water-filled pore space; θ: volumetric water content; ϕ soil porosity; a_+ and b_+ are intercept and slope of linear regression for increasing activity (i.e., $b_+ > 0$); a_- and b_- are intercept and slope of linear regression for decreasing activity (i.e., $b_- < 0$); $WFP_i, (i = 1,2,3,4)$ and a_+, b_+, a_-, b_- are adapted from Muller [58].	(S72)

Table S7. Experimental data for MEND model calibration and validation

Response variable	Description	Objective function	Data points	Weight
Rs	Soil respiration	$1-R^2$	32	0.5
SOC	Soil organic carbon	MAREt, tolerance = 0.05	2	0.2
MBC	Microbial biomass carbon	MAREt, tolerance = 0.1	2	0.3
Microbial C:N	Microbial C:N ratio	|PBIAS|	2	0.4
NH_4^+	Ammonium concentration	|PBIAS|	2	0.3
NO_3^-	Nitrate concentration	|PBIAS|	2	0.3
Microbial CUE	Microbial carbon use efficiency	For model validation only.	1	—
EPO	Oxidase		1	
EPH	Hydrolase		1	

Note: R^2 is the coefficient of determination (Eq. S74), MAREt is the mean absolute relative error (MARE) with a tolerance (Eq. S77), |PBIAS| is the absolute value of the percent bias (Eq. S75).

Table S8. Optimal parameter and objective function values under different weight schemes.

Parameter	W0	W1	W2	W3
r_0	0.38	0.56	0.46	0.48
r_E	0.03	0.03	0.03	0.03
p_{EP}	0.01	0.01	0.01	0.01
fp_{EM}	2.99	2.65	2.73	2.74
V_g	0.017	0.017	0.017	0.017
α	0.5	0.5	0.5	0.5
K_D	0.29	0.28	0.29	0.29
Y_g	0.31	0.33	0.34	0.35
β	7.4	9.9	9.9	9.7
γ	0.0015	0.0018	0.0019	0.0023
VN_{im}	0.099	0.083	0.087	0.085
VN_{fix}	0.099	0.099	0.099	0.099
VN_{nit}	975	959	972	978
VN_{denit}	0.89	0.66	0.66	0.66
VN_{VG}	1e-6	1e-6	1e-6	1e-6
Response variable	f_{OBJ} (calibration | validation), best = 0			
Rs	0.34 | 0.38	0.34 | 0.37	0.34 | 0.38	0.34 | 0.39
SOC	0.33 | 0.31	0.33 | 0.31	0.33 | 0.31	0.33 | 0.31
MBC	0.21 | 0.60	0.17 | 0.66	0.18 | 0.64	0.18 | 0.64
C:N	0.06 | 0.08	0.08 | 0.07	0.07 | 0.07	0.06 | 0.09
NH_4^+	0.42 | 0.43	0.42 | 0.45	0.42 | 0.45	0.42 | 0.45
NO_3^-	0.29 | 0.15	0.30 | 0.13	0.30 | 0.13	0.29 | 0.13

Note: W0 denotes the weighting scheme used in the main text (weights listed in Table S7). W1−W3 are alternative weight schemes. W1 uses weights of 0.5, 0.25, 0.25 for Rs, MBC, and SOC, respectively; and 0.33, 0.33, 0.33 for microbial C:N, NH_4^+, and NO_3^-, respectively. W2: 0.5, 0.2, 0.3 for Rs, MBC, and SOC, respectively; and 0.33, 0.33, 0.33 for microbial C:N, NH_4^+, and NO_3^-, respectively. W3: 0.5, 0.3, 0.2 for Rs, MBC, and SOC; 0.2, 0.4, 0.4 for microbial C:N, NH_4^+, and NO_3^-, respectively.

Supplementary References

1. Wang, G., et al. Microbial dormancy improves development and experimental validation of ecosystem model. *ISME J* **9**, 226-237 (2015).
2. Wang, G., et al. Soil moisture drives microbial controls on carbon decomposition in two subtropical forests. *Soil Biology and Biochemistry* **130**, 185-194 (2019).
3. Wang, G., Post, W. M. & Mayes, M. A. Development of microbial-enzyme-mediated decomposition model parameters through steady-state and dynamic analyses. *Ecological Applications* **23**, 255-272 (2013).
4. Zhou, J., et al. Microbial mediation of carbon-cycle feedbacks to climate warming. *Nat Clim Change* **2**, 106-110 (2012).
5. Xue, K., et al. Tundra soil carbon is vulnerable to rapid microbial decomposition under climate warming. *Nat Clim Change* **6**, 595-600 (2016).
6. Thornton, P. E. & Rosenbloom, N. A. Ecosystem model spin-up: Estimating steady state conditions in a coupled terrestrial carbon and nitrogen cycle model. *Ecol Modell* **189**, 25-48 (2005).
7. Bonan, G. B., Hartman, M. D., Parton, W. J. & Wieder, W. R. Evaluating litter decomposition in earth system models with long-term litterbag experiments: an example using the Community Land Model version 4 (CLM4). *Global Change Biol* **19**, 957-974 (2013).
8. Fanin, N., Fromin, N., Barantal, S. & Hättenschwiler, S. Stoichiometric plasticity of microbial communities is similar between litter and soil in a tropical rainforest. *Scientific Reports* **7**, 12498 (2017).
9. Du, Z., et al. Carbon–nitrogen coupling under three schemes of model representation: a traceability analysis. *Geosci Model Dev* **11**, 4399-4416 (2018).
10. Mooshammer, M., Wanek, W., Zechmeister-Boltenstern, S. & Richter, A. A. Stoichiometric imbalances between terrestrial decomposer communities and their resources: mechanisms and implications of microbial adaptations to their resources. *Front Microbiol* **5**, Article 22 (2014).
11. Mooshammer, M., et al. Adjustment of microbial nitrogen use efficiency to carbon: nitrogen imbalances regulates soil nitrogen cycling. *Nat Commun* **5**, 3694 (2014).
12. Zechmeister-Boltenstern, S., et al. The application of ecological stoichiometry to plant–microbial–soil organic matter transformations. *Ecol Monogr* **85**, 133-155 (2015).
13. Schimel, J. P. & Weintraub, M. N. The implications of exoenzyme activity on microbial carbon and nitrogen limitation in soil: a theoretical model. *Soil Biol Biochem* **35**, 549-563 (2003).
14. Cleveland, C. C. & Liptzin, D. C : N : P stoichiometry in soil: is there a "Redfield ratio" for the microbial biomass? *Biogeochemistry* **85**, 235-252 (2007).
15. Johnson, K. A. & Goody, R. S. The original Michaelis constant: Translation of the 1913 Michaelis–Menten Paper. *Biochemistry* **50**, 8264-8269 (2011).
16. Wang, G. & Post, W. M. A note on the reverse Michaelis–Menten kinetics. *Soil Biol Biochem* **57**, 946-949 (2013).

17. Wang, G. & Post, W. M. A theoretical reassessment of microbial maintenance and implications for microbial ecology modeling. *FEMS Microbiol Ecol* **81**, 610-617 (2012).
18. Wang, G., Mayes, M. A., Gu, L. & Schadt, C. W. Representation of dormant and active microbial dynamics for ecosystem modeling. *PLoS One* **9**, e89252 (2014).
19. Stolpovsky, K., Martinez-Lavanchy, P., Heipieper, H. J., Van Cappellen, P. & Thullner, M. Incorporating dormancy in dynamic microbial community models. *Ecol Modell* **222**, 3092-3102 (2011).
20. Jian, S., et al. Soil extracellular enzyme activities, soil carbon and nitrogen storage under nitrogen fertilization: A meta-analysis. *Soil Biol Biochem* **101**, 32-43 (2016).
21. Sinsabaugh, R. L., et al. Extracellular enzyme kinetics scale with resource availability. *Biogeochemistry* **121**, 287-304 (2014).
22. Fiencke, C. & Bock, E. Immunocytochemical localization of membrane-bound ammonia monooxygenase in cells of ammonia oxidizing bacteria. *Arch Microbiol* **185**, 99-106 (2006).
23. Schlesier, J., Rohde, M., Gerhardt, S. & Einsle, O. A conformational switch triggers nitrogenase protection from oxygen damage by Shethna protein II (FeSII). *J Am Chem Soc* **138**, 239-247 (2016).
24. Song, H.-S., et al. Regulation-structured dynamic metabolic model provides a potential mechanism for delayed enzyme response in denitrification process. *Front Microbiol* **8**, 1866 (2017).
25. Sinsabaugh, R. L., Manzoni, S., Moorhead, D. L. & Richter, A. Carbon use efficiency of microbial communities: stoichiometry, methodology and modelling. *Ecol Lett* **16**, 930-939 (2013).
26. Spohn, M. Microbial respiration per unit microbial biomass depends on litter layer carbon-to-nitrogen ratio. *Biogeosciences* **12**, 817-823 (2015).
27. Tang, J. Y. & Riley, W. J. A total quasi-steady-state formulation of substrate uptake kinetics in complex networks and an example application to microbial litter decomposition. *Biogeosciences* **10**, 8329-8351 (2013).
28. Carvalho, T. L. G., Balsemão-Pires, E., Saraiva, R. M., Ferreira, P. C. G. & Hemerly, A. S. Nitrogen signalling in plant interactions with associative and endophytic diazotrophic bacteria. *Journal of Experimental Botany* **65**, 5631-5642 (2014).
29. Zhu, X., Burger, M., Doane, T. A. & Horwath, W. R. Ammonia oxidation pathways and nitrifier denitrification are significant sources of N2O and NO under low oxygen availability. *Proc Natl Acad Sci USA* **110**, 6328-6333 (2013).
30. Wrage-Mönnig, N., et al. The role of nitrifier denitrification in the production of nitrous oxide revisited. *Soil Biol Biochem* **123**, A3-A16 (2018).
31. Fernando, W., Xia, K. & Rice, C. W. Sorption and desorption of ammonium from liquid swine waste in soils. *Soil Sci Soc Am J* **69**, 1057-1065 (2005).
32. Neitsch, S. L., Arnold, J. G., Kiniry, J. R. & Williams, J. R. Soil and Water Assessment Tool Theoretical Documentation. Version 2009.). Texas Water Resources Institute, Texas A&M University System (2011).
33. Jones, S. B., Or, D. & Bingham, G. E. Gas diffusion measurement and modeling in coarse-textured porous media. *Vadose Zone Journal* **2**, 602-610 (2003).

34. Potter, C. S., Davidson, E. A. & Verchot, L. V. Estimation of global biogeochemical controls and seasonality in soil methane consumption. *Chemosphere* **32**, 2219-2246 (1996).
35. Wang, G. & Chen, S. Evaluation of a soil greenhouse gas emission model based on Bayesian inference and MCMC: Model uncertainty. *Ecol Modell* **253**, 97-106 (2013).
36. Kurylyk, B. L. & Hayashi, M. Improved Stefan equation correction factors to accommodate sensible heat storage during soil freezing or thawing. *Permafrost and Periglacial Processes* **27**, 189-203 (2016).
37. Li, X. & Koike, T. Frozen soil parameterization in SiB2 and its validation with GAME-Tibet observations. *Cold Regions Science and Technology* **36**, 165-182 (2003).
38. Gao, J., et al. A new frozen soil parameterization including frost and thaw fronts in the Community Land Model. *Journal of Advances in Modeling Earth Systems* **11**, 659-679 (2019).
39. Hayes, D. J., et al. The impacts of recent permafrost thaw on land–atmosphere greenhouse gas exchange. *Environmental Research Letters* **9**, 045005 (2014).
40. Liu, L., et al. Permafrost degradation diminishes terrestrial ecosystem carbon sequestration capacity on the Qinghai-Tibetan Plateau. *Global Biogeochemical Cycles* **36**, e2021GB007068 (2022).
41. Feng, X., Nielsen, L. L. & Simpson, M. J. Responses of soil organic matter and microorganisms to freeze–thaw cycles. *Soil Biology and Biochemistry* **39**, 2027-2037 (2007).
42. Kicklighter, D. W., Melillo, J. M., Monier, E., Sokolov, A. P. & Zhuang, Q. Future nitrogen availability and its effect on carbon sequestration in Northern Eurasia. *Nature communications* **10**, 3024 (2019).
43. Liang, J., et al. Biotic responses buffer warming-induced soil organic carbon loss in Arctic tundra. *Global Change Biology* **24**, 4946-4959 (2018).
44. Meisner, A., et al. Soil microbial legacies differ following drying-rewetting and freezing-thawing cycles. *The ISME Journal* **15**, 1207-1221 (2021).
45. Jansson, J. K. & Taş, N. The microbial ecology of permafrost. *Nature Reviews Microbiology* **12**, 414-425 (2014).
46. Nikrad, M. P., Kerkhof, L. J. & Häggblom, M. M. The subzero microbiome: microbial activity in frozen and thawing soils. *FEMS Microbiology Ecology* **92**, fiw081 (2016).
47. Lennon, J. T. & Jones, S. E. Microbial seed banks: the ecological and evolutionary implications of dormancy. *Nature Reviews Microbiology* **9**, 119-130 (2011).
48. Wang, G., Post, W. M., Mayes, M. A., Frerichs, J. T. & Jagadamma, S. Parameter estimation for models of ligninolytic and cellulolytic enzyme kinetics. *Soil Biol Biochem* **48**, 28-38 (2012).
49. Devevre, O. C. & Horwath, W. R. Decomposition of rice straw and microbial carbon use efficiency under different soil temperatures and moistures. *Soil Biol Biochem* **32**, 1773-1785 (2000).
50. Tucker, C. L., Bell, J., Pendall, E. & Ogle, K. Does declining carbon-use efficiency explain thermal acclimation of soil respiration with warming? *Global Change Biol* **19**, 252-263 (2013).
51. Frey, S. D., Lee, J., Melillo, J. M. & Six, J. The temperature response of soil microbial

efficiency and its feedback to climate. *Nat Clim Change* **3**, 395-398 (2013).
52. Steinweg, J. M., Plante, A. F., Conant, R. T., Paul, E. A. & Tanaka, D. L. Patterns of substrate utilization during long-term incubations at different temperatures. *Soil Biol Biochem* **40**, 2722-2728 (2008).
53. Fieschko, J. & Humphrey, A. E. Statistical analysis in the estimation of maintenance and true growth yield coefficients. *Biotechnol Bioeng* **26**, 394-396 (1984).
54. Steinweg, J. M., Dukes, J. S. & Wallenstein, M. D. Modeling the effects of temperature and moisture on soil enzyme activity: Linking laboratory assays to continuous field data. *Soil Biol Biochem* **55**, 85-92 (2012).
55. Hansen, S., Jensen, H. E., Nielsen, N. E. & Svendsen, H. DAISY-Soil plant atmosphere system model.). The Royal Veterinary and Agricultural University (1990).
56. Manzoni, S., Schimel, J. P. & Porporato, A. Responses of soil microbial communities to water stress: results from a meta-analysis. *Ecology* **93**, 930-938 (2012).
57. Manzoni, S., Schaeffer, S. M., Katul, G., Porporato, A. & Schimel, J. P. A theoretical analysis of microbial eco-physiological and diffusion limitations to carbon cycling in drying soils. *Soil Biol Biochem* **73**, 69-83 (2014).
58. Muller, C. *Modeling soil-biosphere interactions*. CABI Publishing (1999).
59. Chen, Y., et al. Whole-soil warming leads to substantial soil carbon emission in an alpine grassland. *Nature Communications* **15**, 4489 (2024).
60. Yuan, X., et al. Sensitivity of soil carbon dynamics to nitrogen and phosphorus enrichment in an alpine meadow. *Soil Biology and Biochemistry* **150**, (2020).
61. van Genuchten, M. T. A closed-form equation for predicting the hydraulic conductivity of unsaturated soils. *Soil Sci Soc Am J* **44**, 892-898 (1980).
62. Tuller, M. & Or, D. Retention of water in soil and the soil water characteristic curve. *Encyclopedia of Soils in the Environment* **4**, 278-289 (2004).
63. Liang, J., et al. Evaluating the E3SM Land Model version 0 (ELMv0) at a temperate forest site using flux and soil water measurements. *Geoscientific Model Development* **12**, 1601-1612 (2019).
64. Zhang, Q., et al. Whole-soil-profile warming does not change microbial carbon use efficiency in surface and deep soils. *Proceedings of the National Academy of Sciences* **120**, e2302190120 (2023).
65. Refsgaard, J. C. Parameterisation, calibration and validation of distributed hydrological models. *J Hydrol* **198**, 69-97 (1997).
66. Wang, G. & Chen, S. A review on parameterization and uncertainty in modeling greenhouse gas emissions from soil. *Geoderma* **170**, 206-216 (2012).
67. Conover, W. J. *Practical Nonparametric Statistics, 3rd Edition*. John Wiley & Sons (1998).
68. Zhang, X. Y., Trame, M., Lesko, L. & Schmidt, S. Sobol sensitivity analysis: a tool to guide the development and evaluation of systems pharmacology models. *CPT: pharmacometrics & systems pharmacology* **4**, 69-79 (2015).
69. Duan, Q. Y., Sorooshian, S. & Gupta, V. Effective and efficient global optimization for conceptual rainfall-runoff models. *Water Resour Res* **28**, 1015-1031 (1992).
70. Wang, G., Jager, H. I., Baskaran, L. M. & Brandt, C. C. Hydrologic and water quality responses to biomass production in the Tennessee River Basin. *Global Change Biol*

Bioenergy **10**, 877-893 (2018).
71. Cleveland, C. C., et al. Global patterns of terrestrial biological nitrogen (N2) fixation in natural ecosystems. *Global Biogeochemical Cycles* **13**, 623-645 (1999).
72. Fisher, J. B., et al. Carbon cost of plant nitrogen acquisition: A mechanistic, globally applicable model of plant nitrogen uptake, retranslocation, and fixation. *Global Biogeochem Cycles* **24**, GB1014 (2010).
73. Reyes, J., et al. Improved estimation of nitrogen uptake in grasslands using the nitrogen dilution curve. *Agronomy for Sustainable Development* **35**, 1561-1570 (2015).
74. Wang, G., Li, W., Wang, K. & Huang, W. Uncertainty quantification of the soil moisture response functions for microbial dormancy and resuscitation. *Soil Biol Biochem* **160**, 108337 (2021).
75. Wang, G., Xia, J. & Chen, J. Quantification of effects of climate variations and human activities on runoff by a monthly water balance model: A case study of the Chaobai River basin in northern China. *Water Resour Res* **45**, W00A11 (2009).
76. Wang, G. & Xia, J. Improvement of SWAT2000 modelling to assess the impact of dams and sluices on streamflow in the Huai River basin of China. *Hydrological Processes* **24**, 1455-1471 (2010).
77. Zhang, X., Srinivasan, R., Zhao, K. & Liew, M. V. Evaluation of global optimization algorithms for parameter calibration of a computationally intensive hydrologic model. *Hydrological Processes* **23**, 430-441 (2009).
78. Duan, Q. Y., Sorooshian, S. & Gupta, V. K. Optimal use of the SCE-UA global optimization method for calibrating watershed models. *J Hydrol* **158**, 265-284 (1994).